Elasticity of nematic phases with fundamental measure theory

René Wittmann, Matthieu Marechal, and Klaus Mecke
Institut für Theoretische Physik, Universität Erlangen-Nürnberg, Staudtstraße 7, D-91058 Erlangen, Germany
(Received 20 February 2015; published 7 May 2015)

In a previous publication [R. Wittmann, M. Marechal, and K. Mecke, Europhys. Lett. **109**, 26003 (2015)], we introduced fundamental mixed measure theory (FMMT) for mixtures of anisotropic hard bodies, which shows that earlier results with an empirical parameter are inaccurate. Now we provide a deeper insight into the background of this theory in integral geometry. We study the Frank elastic coefficients in the nematic phase of the hard spherocylinder fluid. The framework of FMMT provides us with the required direct correlation function without additional input of an equation of state. A series representation of the mixed measure gives rise to closed analytical formulas for the elastic constants that only depend on the density, order parameters, and the particle geometry, pointing out a significant advantage of our geometry-based approach compared to other density functionals. Our elastic coefficients are in good agreement with computer simulations and increase with the density and the nematic order parameter. We confirm earlier mean-field predictions in the limits of low orientational order and infinitely long rods.

DOI: 10.1103/PhysRevE.91.052501 PACS number(s): 61.30.Cz, 61.20.Gy, 61.30.Gd, 64.70.M−

I. INTRODUCTION

The elastic behavior of nematic phases is one of the unique properties that demonstrates the important role of liquid crystals [1] in soft matter [2]. The cost of elastic energy to locally disturb the direction of preferred alignment in this fluidlike state is relatively small compared to the elasticity of a solid. Hence, small external fields are sufficient to penetrate a nematic liquid crystal and thereby tune its birefringence, which is the key principle used to control visual displays [3].

In the famous continuum model introduced by Frank in 1958, the uniaxial nematic director $\hat{n}(\mathbf{r})$ is considered as a unit vector field [4]. The elastic free energy,

$$\Delta F = \frac{1}{2}\int d\mathbf{r}(K_1(\nabla\cdot\hat{n})^2 + K_2(\hat{n}\cdot(\nabla\times\hat{n}))^2 + K_3(\hat{n}\times(\nabla\times\hat{n}))^2), \quad (1)$$

accounts for all sorts of curvature elasticity in the nematic bulk liquid on the basis of three distinct deformations of the director field, neglecting surface terms. The elastic coefficients K_ϵ, with $\epsilon\in\{1,2,3\}$, are assigned to quantify the increase of the free energy which corresponds to a specific distortion, namely, splay, twist, and bend. These phenomenological parameters can be measured in experiments [5–8] or determined for a model system, which is the goal of this article introducing a microscopic theory.

In 1949, Onsager [9] showed that a fluid consisting of hard bodies, which only interact through entropic excluded-volume effects, is a suitable model for liquid crystals [10]. Using Onsager's second-virial approximation and appropriate trial functions for the orientational distribution yields numeric values for the elastic coefficients of infinitely long rods [11,12]. Priest found a general expansion for ratios of the elastic coefficients in terms of ratios of the nematic order parameters [13]. In the limit of low order, there are only two distinct elastic constants, as $K_1 = K_3$. This result agrees with with Landau-de Gennes theory [14], which considers at least squared gradient terms in the nematic order parameter. The two elastic parameters account for the symmetry of the isotropic phase. A more general mean-field calculation yields the relations $K_3 > K_1 > K_2$ for rodlike and $K_2 > K_1 > K_3$ for disklike mesogens [15].

Density functional theory (DFT) constitutes a framework to study inhomogeneous systems [16]. In 1979, Poniewierski and Stecki [17,18] developed a general approach to calculate the elastic coefficients

$$\beta K_\epsilon = \frac{1}{2}\int d\mathbf{r}d\varpi d\varpi' r_\epsilon^2\, c^{(2)}(\mathbf{r},\varpi,\varpi') \times \rho'(\hat{n}\cdot\hat{\varpi})\rho'(\hat{n}\cdot\hat{\varpi}')\hat{\varpi}_x\hat{\varpi}_x', \quad (2)$$

where $\epsilon\in\{1,2,3\}$, via the direct pair correlation function (DCF) $c^{(2)}(\mathbf{r},\varpi,\varpi')$, characterizing the structure of the liquid. This function depends on the distance $\mathbf{r} = (x,y,z) = (r_1,r_2,r_3)$ of two bodies and their uniaxial orientations $\varpi = (\theta,\phi)$, where $\hat{\varpi} = (\hat{\varpi}_x,\hat{\varpi}_y,\hat{\varpi}_z)$ denotes the orientational unit vector. The integrals over $d\varpi$ denote averages over all possible azimuthal angles θ and polar angles ϕ. The derivative of the orientation-dependent density $\rho(\hat{n}\cdot\varpi)$ can be easily obtained using any density functional. Note that there are equivalent representations for K_1 when we substitute $\hat{\varpi}_x\to\hat{\varpi}_y$ and $r_1\to r_2$ and for K_2 with $\hat{\varpi}_x\to\hat{\varpi}_y$ and $r_2\to r_1$.

Poniewierski and Stecki evaluated their equations within the second-virial approximation [17], where the Mayer function constitutes the DCF, later including an attraction term to examine the temperature dependence [18]. In an early extension of Onsager's approach, Parsons [19] introduced a density-dependent prefactor to the Mayer function, which is related to the Carnahan-Starling equation of state for hard spheres [20]. This approach results in a better approximation for the DCF and elastic coefficients of shorter rods [21]. Somoza and Tarazona [22,23] and Poniewierski and Hołyst [24] use similar assumptions in their more advanced weighted-density functionals, which mark further improvements in the theory for elastic coefficients.

Despite the simplicity of the Poniewierski-Stecki equations, their solution remains an interesting problem, as there is no exactly known DCF for a system of anisotropic particles. The density functionals [21–24] applied so far, and therefore also

the resulting expressions for the nematic DCF, involve *ad hoc* approximations. There are some analytic representations of an isotropic reference DCF, extrapolated from results for the hard-sphere fluid [25–28]. The Poniewierski-Stecki equations with these approximations were solved numerically for ellipsoidal particles [29]. Another theoretical method involving the expansion of the isotropic DCF into spherical harmonics gives rise to a series representation for the elastic coefficients [30–32].

Using computer simulations, the elastic coefficients are found from fluctuations of the order tensor in Fourier space. Numerical results are available for hard spherocylinders [33,34], ellipsoids [35,36], and infinitely thin disks [37]. The Poniewierski-Stecki equations from Eq. (2) provide an indirect route to calculate the Frank constants by computer simulation of the DCF [35,36,38]. The elastic coefficients of soft ellipsoids obtained from both methods are in good agreement [36], validating the DFT approach by Poniewierski and Stecki. Yet there exists no quantitatively accurate analytical solution to their equations.

With his seminal fundamental measure theory (FMT) for mixtures of hard spheres [39], Rosenfeld initiated a new era in DFT. The framework of FMT brings many advantages compared to ordinary weighted-density functionals, in particular regarding anisotropic bodies. First, the interaction between two hard bodies is purely described by geometric measures, comprised within a set of weighted densities. Second, FMT is derived from first principles, i.e., no knowledge about the phase behavior and correlations needs to be imposed. Such functionals yield a simple analytic representation of the DCF, which is a nontrivial result, as the DCF is not an input of the theory. As a result, the Rosenfeld functional reproduces the equation of state and the DCF obtained from the Percus-Yevick integral equation theory [40,41]. Finally, the functional can be easily refined without changing the internal structure, meaning the definition of the weighted densities, and therefore the strategy to calculate the DCF. For example, a modification of FMT [42,43] outputs the equation of state derived by Carnahan and Starling [20] for monodisperse hard spheres, which is more accurate than the Percus-Yevick result. The resulting DCF was used to construct a new version for anisotropic bodies [25], which yields better results for the elastic coefficients than approximations solely based on the Percus-Yevick DCF [29].

Although the FMT functional in its original form fails to describe nematic order [44,45], the extension to mixtures of anisotropic bodies is quite natural, introducing additional tensorial weight functions [46,47]. For an efficient calculation, the usual practice is to introduce an empirical parameter [46–50] or perform a more sophisticated systematic expansion [51]. The earlier functionals for mixtures of spheres and infinitely thin rods and disks [52] or parallel cylinders [53,54] were derived with more specific assumptions.

An important requirement for all FMT-like functionals is the crossover to an appropriate expression for the free energy in lower dimensions, i.e., in extreme confinement. Rosenfeld's original functional, which lacks a correct dimensional crossover, needs to be modified to describe a stable hard-sphere crystal [55,56]. Later, a consistent version of the functional was systematically derived from zero-dimensional cavities [57,58]. For anisotropic bodies, this issue becomes even more delicate [48,51]. The limit of extreme anisotropy gives rise to further constraints [51], which exclude Tarazona's most recent expression [58] for hard spheres, also proposed for anisotropic FMT [46]. The violation of these constraints also reflects itself in an unstable smectic-A phase. Our results [51] using the version of FMT by Tarazona and Rosenfeld [57] do show the qualitatively correct behavior of the nematic–smectic-A transition when, in addition, the empirical parameter is chosen appropriately.

In this paper, we continue our discussion of fundamental mixed measure theory (FMMT) and its derivation from integral geometry [59]. The arguments from our earlier publication [59] in favor of using this advanced generalization of FMT rather than the simpler version are as follows. (i) FMMT is the first version of FMT for nonspherical particles that is exact up to quadratic order in the packing fraction η for any density profile and, as a result, in the Onsager limit of infinite rod aspect ratio, $l \to \infty$, at finite ηl. (ii) Relatedly, it yields a good description of both the isotropic-nematic and the nematic–smectic-A transition [59]. (iii) The quantitative results for the isotropic-nematic interfacial tension are excellent [59]. It is not possible to achieve this accuracy consistently for all rod lengths with the computationally cheaper FMT [51] that involves a (fixed) semiempirical parameter.

To carry on the evaluation of FMMT, we calculate the Frank elastic coefficients of the nematic phase. Inserting the provided DCF into Eq. (2), we derive the explicit expressions

$$\beta K_\epsilon = -\frac{\rho^2}{2}\sum_{\nu,\mu}\frac{\partial^2\Phi_{\mathrm{ex}}}{\partial n_\nu \partial n_\mu}\mathcal{T}_\epsilon[\omega^{(\nu)}\otimes\omega^{(\mu)}] - \rho^2\sum_{\upsilon}\frac{\partial\Phi_{\mathrm{ex}}}{\partial N_{12}^{(\upsilon)}}\mathcal{T}_\epsilon\big[\Omega_{(\upsilon)}^{(1\otimes 2)}\big]. \tag{3}$$

Hence, we only need to calculate partial derivatives of the excess free energy density Φ_{ex} with respect to its building blocks, which are different weighted densities n_ν and mixed weighted densities $N_{12}^{(\upsilon)}$, and evaluate the functionals $\mathcal{T}_\epsilon$ of convolution products of the associated weight functions $\omega^{(\nu)}$ and mixed weight function $\Omega_{(\upsilon)}$. As the FMMT functional, these formulas are exact up to quadratic order in the density. Using a series representation, we can calculate all expressions in Eq. (3) analytically for hard spherocylinders and, we expect, also for other simple convex particle shapes that form uniaxial nematic phases. The closed analytic formulas, which we provide in Sec. III C and Appendix B, are in good agreement with the numerical FMMT result at infinite order and the elastic constants measured in computer simulations.

The paper is arranged as follows. In the first part, Sec. II, we derive the theory in its most general form, i.e., for mixtures of arbitrary convex particles. We explore the foundation of FMT functionals in integral geometry, consider different approximate variants of our new theory, and provide the general recipe to obtain the DCF. In the second part, we restrict ourselves to a monodisperse fluid of uniaxial hard spherocylinders, with the orientation dependence as in Eq. (2). We calculate the elastic coefficients from the Poniewierski-Stecki equations via Eq. (3), which we explain in detail in Sec. III. We discuss our analytical and numerical results in comparison

with previous work. In Sec. IV, we draw conclusions regarding the theoretical approach and applications of our analytical formulas.

II. FUNDAMENTAL MIXED MEASURE THEORY

Based on recent developments in translative integral geometry, we proposed a new generalization of FMT for anisotropic hard bodies [59]. Here, we derive this FMMT with a greater focus on the mathematical concepts and the proposed series representations. In Sec. II A, we review the framework of DFT and introduce the Rosenfeld functional for hard spheres. We draw parallels between FMT functionals and measures from integral geometry in Sec. II B. We introduce the translative integral formula, which we use in Sec. II C to derive an alternative decomposition of the Mayer f function and find an additional building block of FMT based on a mixed measure of two bodies. In Sec. II D, we provide the full expression for this new functional and explore its relation to the representation in terms of tensorial measures [46,47]. We further calculate the related direct correlation functions.

A. Rosenfeld's fundamental measure theory

Fluids of hard bodies are of particular interest for theorists, as we can describe their purely repulsive pair interaction exclusively in terms of geometrical quantities. Integral geometry [60] is the foundation of many sophisticated density functionals for hard bodies, from the work of Onsager [9], who considered the excluded volume of two infinitely long rods, to Rosenfeld's FMT [39] and its generalizations [46,59].

The central task in DFT is to find a functional $\Omega[\{\rho_i\}]$ which is equal to the grand potential Ω in equilibrium and has a larger value otherwise [16]. The equilibrium profile $\rho_i(\mathcal{R})$ of the number density of species i follows from the variational principle $\delta\Omega/\delta\rho_i(\mathcal{R}) = 0$ for any external potential $V_i^{\text{ext}}(\mathcal{R})$. In an anisotropic fluid, the density depends on position $\mathbf{r}$ and orientation $\mathbf{O}$, shortly $\mathcal{R} = (\mathbf{r},\mathbf{O})$. For a system with κ components, the general functional reads

$$\Omega[\{\rho_i\}] = \mathcal{F}[\{\rho_i\}] + \sum_{i=1}^{\kappa} \int d\mathcal{R}\rho_i(\mathcal{R})\big(V_i^{\text{ext}}(\mathcal{R}) - \mu_i\big), \quad (4)$$

where μ_i are the chemical potentials and $\int d\mathcal{R} = \int d\mathbf{r} \int d\mathbf{O}$ includes the spatial integration and the orientational average. We may separate the orientation dependence of the density profile $\rho(\mathcal{R}) = \rho(\mathbf{r})g(\mathbf{r},\mathbf{O})$ into an explicit orientational distribution $g(\mathbf{r},\mathbf{O})$. The intrinsic free energy

$$\beta\mathcal{F}[\{\rho_i\}] = \beta\mathcal{F}_{\text{id}} + \beta\mathcal{F}_{\text{ex}} = \int d\mathbf{r}(\Phi_{\text{id}}(\mathbf{r}) + \Phi_{\text{ex}}(\mathbf{r})) \quad (5)$$

in Eq. (4) has the ideal gas contribution

$$\Phi_{\text{id}}(\mathbf{r}) = \sum_{i=1}^{\kappa} \rho_i(\mathbf{r})[\ln \rho_i(\mathbf{r})\Lambda^3 - 1] + \rho_i(\mathbf{r}) \int d\mathbf{O} g_i(\mathbf{r},\mathbf{O}) \ln g_i(\mathbf{r},\mathbf{O}), \quad (6)$$

where Λ is the thermal wavelength, $\beta^{-1} = k_B T$ is the inverse temperature, and the functional $\Phi(\mathbf{r})$ is the free energy density. The excess free energy density Φ_{ex}, which contains the explicit information about the interactions in the system, is *a priori* unknown.

The key idea of Rosenfeld's FMT [39] (in three dimensions) is to construct the approximate excess free energy density

$$\Phi_{\text{ex}} = -n_0 \ln(1-n_3) + \frac{n_1 n_2 - \vec{n}_1 \vec{n}_2}{(1-n_3)} + \frac{n_2^3 - 3n_2 \vec{n}_2 \vec{n}_2}{(1-n_3)^2} \quad (7)$$

as a function of weighted densities,

$$n_\nu(\mathbf{r}) = \sum_{i=1}^{\kappa} \int d\mathcal{R}_1 \rho_i(\mathcal{R}_1)\, \omega_i^{(\nu)}(\mathbf{r} - \mathcal{R}_1), \quad (8)$$

where $(\mathbf{r} - \mathcal{R}_1)$ is short for $(\mathbf{r} - \mathbf{r}_1, \mathbf{O}_1)$. The geometry of a single hard sphere is fully contained in the scalar

$$\begin{aligned} \omega_i^{(3)}(\mathbf{r}) &= \Theta\left(|\mathbf{R}_i(\hat{\mathbf{r}})| - |\mathbf{r}|\right), \\ \omega_i^{(2)}(\mathbf{r}) &= \frac{\delta(|\mathbf{R}_i(\hat{\mathbf{r}})| - |\mathbf{r}|)}{\mathbf{n}_i(\hat{\mathbf{r}})\hat{\mathbf{r}}}, \\ \omega_i^{(1)}(\mathbf{r}) &= \frac{H_i(\hat{\mathbf{r}})}{4\pi}\omega_i^{(2)}(\mathbf{r}), \\ \omega_i^{(0)}(\mathbf{r}) &= \frac{K_i(\hat{\mathbf{r}})}{4\pi}\omega_i^{(2)}(\mathbf{r}), \end{aligned} \quad (9)$$

and vectorial

$$\begin{aligned} \vec{\omega}_i^{(2)}(\mathbf{r}) &= \mathbf{n}_i(\hat{\mathbf{r}})\omega_i^{(2)}(\mathbf{r}), \\ \vec{\omega}_i^{(1)}(\mathbf{r}) &= \frac{H_i(\hat{\mathbf{r}})}{4\pi}\vec{\omega}_i^{(2)}(\mathbf{r}), \end{aligned} \quad (10)$$

weight functions, written in the form for a general convex body $\mathcal{B}_i$ of species i. The weight functions $\omega_i^{(\nu)}$ depend on geometrical properties of a convex body centered in the origin. These are the principal κ_i^I and κ_i^{II}, mean $H_i = \frac{1}{2}(\kappa_i^I + \kappa_i^{II})$ and Gaussian $K_i = \kappa_i^I \kappa_i^{II}$ curvature, and the outward normal $\mathbf{n}_i$ on the surface $\partial\mathcal{B}_i$ at $\mathbf{R}_i(\hat{\mathbf{r}})$, where $\hat{\mathbf{r}} = \mathbf{r}/|\mathbf{r}|$ denotes the radial unit vector. The explicit orientation dependence in the weight functions of anisotropic bodies is discussed in Ref. [49]. Now we explore the geometrical background of FMT.

B. Integral geometry in density functional theory

Minkowski functionals [61], which provide a complete basis of any additive, motion-invariant, and conditionally continuous morphometrical functional [62], constitute a sophisticated concept to measure the shape of a convex body $\mathcal{B}_i \subset \mathbb{R}^d$. We use the notational convention of Ref. [60] and consider the equivalent intrinsic volumes $V_\nu(\mathcal{B}_i)$, which are normalized such that their value does not depend on the dimension of the space in which they are embedded. We use the calculus with sets for the translation $\mathbf{r} + \mathcal{B}_i = \mathcal{B}_i + \mathbf{r} := \{\mathbf{r} + \mathbf{x} : \mathbf{x} \in \mathcal{B}_i\}$ by a vector $\mathbf{r} \in \mathbb{R}^d$ and multiplication $a\mathcal{B}_i := \{a\mathbf{x} : \mathbf{x} \in \mathcal{B}_i\}$ of a body $\mathcal{B}_i$ with any real number $a \in \mathbb{R}$. In particular, $-\mathcal{B}_i$ is an abbreviation for $(-1)\mathcal{B}_i$. Finally, we define the Minkowski sum $\mathcal{B}_i \uplus \mathcal{B}_j := \{\mathbf{x} + \mathbf{y} : \mathbf{x} \in \mathcal{B}_i, \mathbf{y} \in \mathcal{B}_j\}$ for two bodies $\mathcal{B}_i, \mathcal{B}_j \subset \mathbb{R}^d$. Writing $v_{\text{excl}} = V_d(\mathcal{B}_i \uplus -\mathcal{B}_j)$ for their mutual excluded volume provides a physical interpretation.

In d dimensions, we define the intrinsic volumes $V_0,\dots,V_{d-1}$ through the Steiner formula

$$V_d(\mathcal{B}_{i,\varrho}) = \sum_{\nu=0}^{d} \varrho^{d-\nu}\kappa_{d-\nu} V_\nu(\mathcal{B}_i) \tag{11}$$

for the d-dimensional volume V_d of the parallel body $\mathcal{B}_{i,\varrho} := \mathcal{B}_i \uplus \varrho B^d$, where ϱB^d denotes the d-dimensional ball of radius ϱ and $\kappa_d = \pi^{d/2}/\Gamma(1+d/2)$ is the volume of the unit ball. In two dimensions we interpret the intrinsic volumes as the shape measures

$$\begin{aligned} a(\mathcal{B}_i) &= V_2(\mathcal{B}_i) && \text{area},\\ l(\mathcal{B}_i) &= 2V_1(\mathcal{B}_i) && \text{perimeter},\\ \chi(\mathcal{B}_i) &= V_0(\mathcal{B}_i) && \text{Euler characteristic}, \end{aligned} \tag{12}$$

and in three dimensions we have

$$\begin{aligned} v(\mathcal{B}_i) &= V_3(\mathcal{B}_i) && \text{volume},\\ s(\mathcal{B}_i) &= 2V_2(\mathcal{B}_i) && \text{surface area},\\ m(\mathcal{B}_i) &= \pi V_1(\mathcal{B}_i) && \text{integral mean curvature},\\ \chi(\mathcal{B}_i) &= V_0(\mathcal{B}_i) && \text{Euler characteristic}. \end{aligned} \tag{13}$$

Note that in the latter case the Euler characteristic $\chi(\mathcal{B}_i)$ is equivalent to the integral Gaussian curvature divided by 4π. See Sec. 14.2 in Ref. [60] for the general expressions in d dimensions.

Consider a Borel set (any set formed from open sets by countable union, countable intersection, and relative complement [60]) $A \subset \mathbb{R}^d$. In generalization of the concept of intrinsic volumes, we introduce the curvature measures $\Phi_\nu(\mathcal{B}_i, A)$, such that $\Phi_\nu(\mathcal{B}_i,\mathbb{R}^d) = V_\nu(\mathcal{B}_i)$. These local measures are defined through the local version [60],

$$\lambda(\mathbf{x} \in \mathcal{B}_{i,\varrho} : \mathbf{p}(\mathcal{B}_i,\mathbf{x}) \in A) = \sum_{\nu=0}^{d} \varrho^{d-\nu}\kappa_{d-\nu}\Phi_\nu(\mathcal{B}_i, A), \tag{14}$$

of the Steiner Formula, Eq. (11). Here $\lambda(\mathbf{x})$ denotes the Lebesgue measure on $\mathbb{R}^d$ and $\mathbf{p}(\mathcal{B}_i,\mathbf{x}) \in \mathcal{B}_i$ is the point in $\mathcal{B}_i$ with the smallest distance to $\mathbf{x}$.

The argument of the weight functions $\omega_i^{(\nu)}(\mathbf{r}-\mathcal{R}_1)$ within the integrand in Eq. (8) depends on two points. As shown in Fig. 1(a), we consider a body $\mathcal{B}_i(\mathcal{R}_1)$ centered at $\mathbf{r}_1$ with orientation $\mathbf{O}_1$, where $\mathbf{r}$ denotes an arbitrary point in space. If $\mathbf{r}$ lies on $\partial\mathcal{B}_i$, then $\mathbf{r}-\mathbf{r}_1$ is equivalent to the vector $\mathbf{R}_i(\widehat{\mathbf{r}-\mathbf{r}_1})$ parametrizing the surface, such that the argument of the δ distribution in Eq. (9) vanishes. For three-dimensional bodies $\mathcal{B}_i$ with a twice differentiable boundary, the curvature measures are related to the four scalar weight functions from Eq. (9) by

$$\mathfrak{c}_\nu\Phi_\nu(\mathcal{B}_i(\mathbf{r}_1,\mathbf{O}_1), A) = \int_A d\mathbf{r}\,\omega_i^{(\nu)}(\mathbf{r}-\mathbf{r}_1,\mathbf{O}_1). \tag{15}$$

The proportional constants $\mathfrak{c}_3 = 1$, $\mathfrak{c}_2 = 2$, $\mathfrak{c}_1 = 1/4$, and $\mathfrak{c}_0 = 1$ follow from the different normalizations; compare the factors $(4\pi)^{-1}$ in Eq. (9) and the relations in Eq. (13) for $A = \mathbb{R}^3$. More precisely, Eq. (15) can be proven by inserting Eq. (9) into its right-hand-side and comparing to the curvature representation of Φ_ν on p. 607 in Ref. [60].

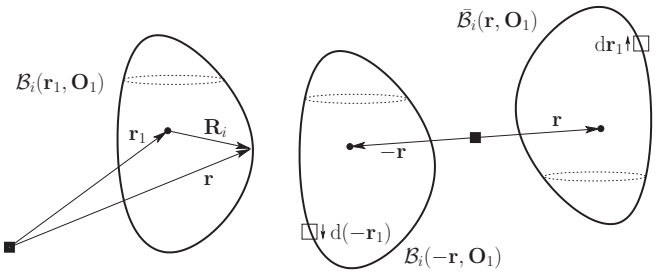

FIG. 1. Oriented bodies $\mathcal{B}_i \subset \mathbb{R}^3$ in a coordinate system. We denote the centers of the bodies by a dot and the origin of the coordinates by a solid square. (a) Illustration of $\mathcal{B}_i(\mathbf{r}_1,\mathbf{O}_1)$ centered at $\mathbf{r}_1$ and parametrized by $\mathbf{R}_i(\widehat{\mathbf{r}-\mathbf{r}_1})$, as used in the weight functions found in Eq. (8). If $\mathbf{r} \in \mathbb{R}^3$ lies on $\partial\mathcal{B}_i(\mathbf{r}_1,\mathbf{O}_1)$, then $\mathbf{R}_i(\widehat{\mathbf{r}-\mathbf{r}_1}) = \mathbf{r}-\mathbf{r}_1$. (b) Comparison of a body $\mathcal{B}_i(-\mathbf{r},\mathbf{O}_1)$ centered at $-\mathbf{r}$ with its inversion $\bar{\mathcal{B}}_i(\mathbf{r},\mathbf{O}_1)$ at $\mathbf{r}$. It can be seen that the elements $d\mathbf{r}_1 \cap \bar{\mathcal{B}}_i(\mathbf{r},\mathbf{O}_1)$ and $d(-\mathbf{r}_1) \cap \mathcal{B}_i(-\mathbf{r},\mathbf{O}_1)$ are each other's image under point reflection.

For an infinitesimally small volume element $A \equiv d\mathbf{r}$, we can write the weight functions as

$$\omega_i^{(\nu)}(\mathbf{r}-\mathbf{r}_1,\mathbf{O}_1)\,d\mathbf{r} = \mathfrak{c}_\nu\Phi_\nu(\mathcal{B}_i(\mathbf{r}_1,\mathbf{O}_1), d\mathbf{r}). \tag{16}$$

Inverting the body $\mathcal{B}_i(\mathbf{r},\mathbf{O}_1)$ at its center $\mathbf{r}$, denoted by $\bar{\mathcal{B}}_i(\mathbf{r},\mathbf{O}_1) := 2\mathbf{r} - \mathcal{B}_i(\mathbf{r},\mathbf{O}_1)$, we find

$$\mathfrak{c}_\nu\Phi_\nu(\bar{\mathcal{B}}_i(\mathbf{r},\mathbf{O}_1), d\mathbf{r}_1) = \omega_i^{(\nu)}(\mathbf{r}-\mathbf{r}_1,\mathbf{O}_1)\,d\mathbf{r}_1 \tag{17}$$

from the identity $\Phi_\nu(\bar{\mathcal{B}}_i(\mathbf{r},\mathbf{O}_1), d\mathbf{r}_1) = \Phi_\nu(\mathcal{B}_i(-\mathbf{r},\mathbf{O}_1), d(-\mathbf{r}_1))$ and Eq. (16). This relation is illustrated in Fig. 1(b), where $d(-\mathbf{r}_1)$ denotes the image of $d\mathbf{r}_1$ under point reflection. Interchanging $\mathbf{r}_1$ and $\mathbf{r}$ in Eq. (16) and comparing to Eq. (17), we see that the scalar weight functions of a point-symmetric particle $\mathcal{B}_i = \bar{\mathcal{B}}_i$ are also point symmetric.

By construction, the low-density limit of the Rosenfeld functional from Eq. (7) provides the excluded volume v_{excl} of two spheres. Defining $V_\nu^{(i)} := V_\nu(R_i B^3)$, we obtain

$$v_{\text{excl}} = V_3^{(1)}V_0^{(2)} + V_0^{(1)}V_3^{(2)} + \tfrac{1}{2}V_2^{(1)}V_1^{(2)} + \tfrac{1}{2}V_1^{(1)}V_2^{(2)} \tag{18}$$

as the special case of the Steiner formula, Eq. (11), in $d = 3$ with $\mathcal{B}_i = R_1 B^3$ a sphere of radius R_1 and $\varrho = R_2$. The factorization into intrinsic volumes is equivalent to Rosenfeld's decomposition in terms of one-body weight functions [39]. The more general principal kinematic formula (Theorem 5.1.3 in Ref. [60]) gives rise to a representation of the orientationally averaged excluded volume or the second-virial coefficient of two anisotropic bodies $\mathcal{B}_i$ and $\mathcal{B}_j$ with the same form as Eq. (18). Therefore, the FMT functional based on the weight functions from Eq. (9) is suitable to describe the isotropic bulk liquid [44,45]. The factorization in Eq. (18) has already been used in a scaled-particle treatment of anisotropic fluids [63]. However, the Minkowski sum of two anisotropic grains cannot be factorized into intrinsic volumes, which explains the failure of Rosenfeld's FMT for orientationally ordered phases.

In an appropriate generalization of Steiner's formula, the Minkowski sum of two convex bodies $\mathcal{B}_i$ and $\mathcal{B}_j$ involves so-called mixed volumes depending on both bodies simultaneously [60]. To define an appropriate weight function for a DFT, we need to consider a relation similar to Eq. (17) and therefore introduce a local equivalent to mixed volumes. The

existence of mixed measures $\Phi^{(\nu)}_{k,d-k}(\mathcal{B}_i,\mathcal{B}_j; A\times B)$ on Borel sets A and B, defined through the *translative integral formula*

$$\int_{\mathbb{R}^3} \Phi_\nu(\mathcal{B}_i\cap(\mathcal{B}_j+\mathbf{x}), A\cap(B+\mathbf{x}))\,d\mathbf{x} = \sum_{k=\nu}^{d} \Phi^{(\nu)}_{k,d-k}(\mathcal{B}_i,\mathcal{B}_j; A\times B), \tag{19}$$

was proven in Theorem 5.2.3 in Ref. [60]. This fundamental equation provides a relation to a curvature measure Φ_ν in d spatial dimensions. The corollary

$$\int_{\mathbb{R}^d}\int_{\mathbb{R}^d} F(\mathbf{x},\mathbf{x}-\mathbf{y})\,\Phi_\nu(\mathcal{B}_i\cap(\mathcal{B}_j+\mathbf{y}),d\mathbf{x})\,d\mathbf{y} = \sum_{k=\nu}^{d}\int_{\mathbb{R}^d\times\mathbb{R}^d} F(\mathbf{x},\mathbf{y})\,\Phi^{(\nu)}_{k,d-k}(\mathcal{B}_i,\mathcal{B}_j; d(\mathbf{x},\mathbf{y})) \tag{20}$$

provides the mathematical foundation of FMMT when setting $\nu=0$ [59].

Mixed measures obey the symmetry relations

$$\Phi^{(0)}_{k,d-k}(\mathcal{B}_i,\mathcal{B}_j; d(\mathbf{r}_1,\mathbf{r}_2)) = \Phi^{(0)}_{d-k,k}(\mathcal{B}_j,\mathcal{B}_i; d(\mathbf{r}_2,\mathbf{r}_1)). \tag{21}$$

As also known for mixed volumes, the mixed measures

$$\Phi^{(0)}_{0,d}(\mathcal{B}_i,\mathcal{B}_j; d(\mathbf{r}_1,\mathbf{r}_2)) = \Phi_0(\mathcal{B}_i,d\mathbf{r}_1)\,\Phi_d(\mathcal{B}_j,d\mathbf{r}_2) \tag{22}$$

for $k=0$ and equivalently $k=d$ factorize to the curvature measures corresponding to Euler characteristic and volume. In two and three dimensions, we have the explicit expressions [64]

$$\Phi^{(0)}_{1,1}(\mathcal{B}_i,\mathcal{B}_j; d(\mathbf{r}_1,\mathbf{r}_2)) = \frac{\arccos(\mathbf{n}_i\mathbf{n}_j)}{2\pi}|\mathbf{n}_i\times\mathbf{n}_j|C_1(\mathcal{B}_i,d\mathbf{r}_1)C_1(\mathcal{B}_j,d\mathbf{r}_2) \tag{23}$$

and

$$\Phi^{(0)}_{1,2}(\mathcal{B}_i,\mathcal{B}_j; d(\mathbf{r}_1,\mathbf{r}_2)) = \frac{\kappa_i^I\left(\mathbf{v}_i^{II}\mathbf{n}_j\right)^2+\kappa_i^{II}\left(\mathbf{v}_i^{I}\mathbf{n}_j\right)^2}{4\pi(1+\mathbf{n}_i\mathbf{n}_j)}C_2(\mathcal{B}_i,d\mathbf{r}_1)C_2(\mathcal{B}_j,d\mathbf{r}_2), \tag{24}$$

with the directions $\mathbf{v}_i^I$ and $\mathbf{v}_i^{II}$ of the principal curvatures and the boundary measure $C_{d-1}(\mathcal{B}_i,A) := 2\Phi_{d-1}(\mathcal{B}_i,A)$. A similar expression was obtained by Wertheim [65] in his local representation of the second-virial coefficient. Wertheim found that his exact formula reduces to Eq. (18) when applied to the isotropic phase but he never applied it within the context of a more general DFT. Now we are at a point where we can express the pair interaction between two anisotropic hard bodies exactly using such mixed measures.

Briefly returning to measures of a single convex hard body, we now introduce another successful geometrical concept applied in statistical physics. In generalization of Minkowski functionals, which are a complete basis for the description of shape, the notion of isometry-covariant Minkowski tensors [66] allows us to quantify anisotropy through the ratio of their largest and smallest eigenvalues. Relatedly, extended deconvolution fundamental measure theory (edFMT) [46,47], based on the tensorial weighted densities

$$\overleftrightarrow{\omega}_i^{(2)}(\mathbf{r}) = \mathbf{n}_i\mathbf{n}_i^{\mathrm{T}}\,\omega_i^{(2)}(\mathbf{r}),$$
$$\overleftrightarrow{\omega}_i^{(1)}(\mathbf{r}) = \frac{\Delta\kappa_i}{4\pi}\left(\mathbf{v}_i^I\mathbf{v}_i^{I\,\mathrm{T}}-\mathbf{v}_i^{II}\mathbf{v}_i^{II\,\mathrm{T}}\right)\omega_i^{(2)}(\mathbf{r}), \tag{25}$$

provides an approximate generalization of FMT. Here $\Delta\kappa_i = \frac{1}{2}(\kappa_i^I-\kappa_i^{II})$ denotes the deviatoric curvature, which vanishes for spheres. With this extension, we can describe the nematic phase of anisotropic hard bodies qualitatively. Moreover, the tensor $\overleftrightarrow{\omega}_i^{(2)}$ is equal to the one introduced to FMT to describe the hard-sphere crystal [57,58], i.e., a state of isotropically shaped particles with positional anisotropy.

Compared to scalar or vectorial measures, the basic feature of tensorial weighted densities is that they show a nontrivial dependence on the orientational distribution $g(\mathbf{O})$ in the homogeneous nematic phase. The equilibrium distribution must minimize the density functional

$$\frac{\delta\Omega}{\delta g(\mathbf{O})} = \int d\mathbf{r}\left\{\rho(\mathbf{r})[\ln g(\mathbf{O})+1]+\frac{\delta\Phi_{\mathrm{ex}}}{\delta g(\mathbf{O})}\right\} = 0. \tag{26}$$

Without tensorial (or mixed) measures, the variational derivative $\delta\Phi_{\mathrm{ex}}/\delta g(\mathbf{O})$ vanishes trivially, explaining the unsatisfactory description of orientational order within the original FMT. Therefore, we expound a new route to derive the most general version of FMT for arbitrarily shaped convex hard bodies.

C. Decomposition of the Mayer f function

To obtain an accurate version of FMT, we must provide an exact free energy functional,

$$\beta\mathcal{F}_{\mathrm{ex}} \to -\frac{1}{2}\sum_{i,j=1}^{\kappa}\iint d\mathcal{R}_1 d\mathcal{R}_2\rho_i(\mathcal{R}_1)\rho_j(\mathcal{R}_2)f_{ij}(\mathcal{R}_1,\mathcal{R}_2), \tag{27}$$

in the dilute limit, where the average number density $\rho_i\to 0$ of each species vanishes, such that only pair interactions are relevant. The first step is to decompose the characteristic Mayer f function

$$f_{ij}(\mathcal{R}_1,\mathcal{R}_2) = e^{-\beta U_{ij}}-1 = \begin{cases} 0 & \text{if } \mathcal{B}_i\cap\mathcal{B}_j=\emptyset,\\ -1 & \text{if } \mathcal{B}_i\cap\mathcal{B}_j\neq\emptyset,\end{cases} \tag{28}$$

where $U_{ij}(\mathcal{R}_1,\mathcal{R}_2)$ is the pair interaction potential between two hard bodies $\mathcal{B}_i$ and $\mathcal{B}_j$. We see that the interaction only depends on whether the intersection

$$\mathcal{I}_{ij}(\mathcal{R}_1,\mathcal{R}_2) := \mathcal{B}_i(\mathcal{R}_1)\cap\mathcal{B}_j(\mathcal{R}_2) \tag{29}$$

is the empty set $\emptyset$ or not. With this geometric point of view, we find the (local) representation of the Mayer function,

$$-f_{ij}(\mathcal{R}_1,\mathcal{R}_2) = \chi(\mathcal{I}_{ij}) = V_0(\mathcal{I}_{ij}) = \int_{\mathbb{R}^3}\Phi_0(\mathcal{I}_{ij},d\mathbf{r}), \tag{30}$$

in terms of the curvature measure Φ_0. Note that in this step we need to restrict ourselves to convex bodies whose intersection region is simply connected, ensuring that the Euler characteristic $\chi(\mathcal{I}_{ij})=1$ whenever $\mathcal{I}_{ij}\neq\emptyset$.

Inserting f_{ij} from Eq. (30) into Eq. (27), we find

$$\beta\mathcal{F}_{\text{ex}} \to \frac{1}{2}\sum_{i,j=1}^{\kappa}\iiint d\mathcal{R}_1 d\mathcal{R}_2 \rho_i(\mathcal{R}_1)\rho_j(\mathcal{R}_2)\Phi_0(\mathcal{I}_{ij},d\mathbf{r}). \tag{31}$$

Now we apply the translative integral formula from Eq. (20) with $\nu = 0$ to transform the integrand

$$\begin{aligned}
&\iint d\mathbf{r}_1 d\mathbf{r}_2 \rho_i(\mathbf{r}_1)\rho_j(\mathbf{r}_2)\int \Phi_0(\mathcal{I}_{ij}(\mathbf{r}_1,\mathbf{r}_2),d\mathbf{r})\\
&= \iint d\mathbf{x}d\mathbf{y}\rho_i(\mathbf{x})\rho_j(\mathbf{x}-\mathbf{y})\int \Phi_0(\mathcal{I}_{ij}(\mathbf{x},\mathbf{x}-\mathbf{y}),d\mathbf{r})\\
&= \int d\mathbf{r}\iint d\mathbf{y}\rho_i(\mathbf{x})\rho_j(\mathbf{x}-\mathbf{y})\Phi_0(\bar{\mathcal{I}}_{ij}(\mathbf{r},\mathbf{r}+\mathbf{y}),d\mathbf{x})\\
&= \int d\mathbf{r}\sum_{k=0}^{d}\iint \rho_i(\mathbf{x})\rho_j(\mathbf{y})\Phi^{(0)}_{k,d-k}(\bar{\mathcal{B}}_i(\mathbf{r}),\bar{\mathcal{B}}_j(\mathbf{r});d(\mathbf{x},\mathbf{y}))
\end{aligned} \tag{32}$$

in Eq. (27), which is valid for each pair of orientations $\mathbf{O}_1,\mathbf{O}_2$. In the second step, we applied the identity

$$\Phi_\nu(\mathcal{I}_{ij}(\mathbf{x},\mathbf{x}-\mathbf{y}),d\mathbf{r})d\mathbf{x} = \Phi_\nu(\bar{\mathcal{I}}_{ij}(\mathbf{r},\mathbf{r}+\mathbf{y}),d\mathbf{x})d\mathbf{r} \tag{33}$$

for the curvature measures, derived in Appendix A, to the intersection $\mathcal{I}_{ij}(\mathbf{x},\mathbf{x}-\mathbf{y})$, which is also a convex body. The inversion $\bar{\mathcal{I}}_{ij} = \bar{\mathcal{B}}_i \cap \bar{\mathcal{B}}_j$ denotes the intersection of the two bodies inverted at their respective centers. Comparing Eq. (32) with Eq. (27), we find the decomposition

$$\begin{aligned}
&-f_{ij}(\mathcal{R}_1,\mathcal{R}_2)d\mathbf{r}_1 d\mathbf{r}_2\\
&= \int d\mathbf{r}\sum_{k=0}^{d}\Phi^{(0)}_{k,d-k}(\bar{\mathcal{B}}_i(\mathbf{r},\mathbf{O}_1),\bar{\mathcal{B}}_j(\mathbf{r},\mathbf{O}_2);d(\mathbf{r}_1,\mathbf{r}_2))
\end{aligned} \tag{34}$$

of the Mayer f function into the mixed measures $\Phi^{(0)}_{k,d-k}$. We define the mixed weight functions

$$\begin{aligned}
&\Omega^{(k,d-k)}_{ij}(\mathbf{r}-\mathbf{r}_1,\mathbf{r}-\mathbf{r}_2,\mathbf{O}_1,\mathbf{O}_2)d\mathbf{r}_1 d\mathbf{r}_2\\
&\quad := \Phi^{(0)}_{k,d-k}(\bar{\mathcal{B}}_i(\mathbf{r},\mathbf{O}_1),\bar{\mathcal{B}}_j(\mathbf{r},\mathbf{O}_2);d(\mathbf{r}_1,\mathbf{r}_2))
\end{aligned} \tag{35}$$

in analogy to Eq. (17) and obtain

$$-f_{ij}(\mathbf{r},\mathbf{O}_1,\mathbf{O}_2) = \int d\mathbf{r}'\sum_{k=0}^{d}\Omega^{(k,d-k)}_{ij}(\mathbf{r}'-\mathcal{R}_1,\mathbf{r}'-\mathcal{R}_2), \tag{36}$$

where $\mathbf{r} = \mathbf{r}_1 - \mathbf{r}_2$. As a short notation, we further introduced the self-convolution product

$$\Omega^{(k\otimes d-k)}_{ij} = \int d\mathbf{r}'\Omega^{(k,d-k)}_{ij}(\mathbf{r}'-\mathcal{R}_1,\mathbf{r}'-\mathcal{R}_2) \tag{37}$$

of the mixed weight function $\Omega^{(k,d-k)}_{ij}$.

We turn to $d = 3$ dimensions and find the explicit expression for mixed weight function

$$\Omega^{(12)}_{ij}(\mathcal{R}_1,\mathcal{R}_2) = \frac{\kappa^I_i\left(\mathbf{v}^{II}_i\mathbf{n}_j\right)^2 + \kappa^{II}_i\left(\mathbf{v}^{I}_i\mathbf{n}_j\right)^2}{4\pi(1+\mathbf{n}_i\mathbf{n}_j)}\omega^{(2)}_i\omega^{(2)}_j, \tag{38}$$

comparing Eqs. (24) and (35) and applying Eq. (17) to replace the boundary measure $C_2(\bar{\mathcal{B}}_i,d\mathbf{r}_1)$ with the weight function $\omega^{(2)}_i$ from Eq. (9). Following Eq. (22), we can factorize the mixed measures $\Phi^{(0)}_{0,3}$ and $\Phi^{(0)}_{3,0}$ into curvature measures and further recover the scalar weight functions $\omega^{(0)}_i$ and $\omega^{(3)}_i$. Hence, the exact decomposition of the Mayer function reads

$$-f_{ij}(\mathbf{r},\mathbf{O}_1,\mathbf{O}_2) = \omega^{(0)}_i\otimes\omega^{(3)}_j + \Omega^{(1\otimes 2)}_{ij} + (i\leftrightarrow j), \tag{39}$$

where

$$\omega^{(\nu)}_i\otimes\omega^{(\mu)}_j = \int d\mathbf{r}'\omega^{(\nu)}_i(\mathbf{r}'-\mathcal{R}_1)\omega^{(\mu)}_j(\mathbf{r}'-\mathcal{R}_2) \tag{40}$$

denotes the convolution product of the orientation-dependent weight functions from Ref. [46]. Note that we took advantage of the relation from Eq. (21), taking into account the terms with $k \geqslant d/2$ in Eq. (34) by adding the same expression with exchanged indices i and j, denoted by $(i\leftrightarrow j)$. In particular, we used $\Omega^{(12)}_{ji} = \Omega^{(21)}_{ij}$.

Now we use the relation

$$\begin{aligned}
&\kappa^I_i\left(\mathbf{v}^{II}_i\mathbf{n}_j\right)^2 + \kappa^{II}_i\left(\mathbf{v}^{I}_i\mathbf{n}_j\right)^2\\
&\quad = -\Delta\kappa_i\left[\left(\mathbf{v}^{I}_i\mathbf{n}_j\right)^2 - \left(\mathbf{v}^{II}_i\mathbf{n}_j\right)^2\right] + H_i[1-(\mathbf{n}_i\mathbf{n}_j)^2],
\end{aligned} \tag{41}$$

arising from the orthonormality of the unit vectors on the particle's surface, to obtain a different representation

$$\begin{aligned}
\Omega^{(12)}_{ij}(\mathcal{R}_1,\mathcal{R}_2) &= \omega^{(1)}_i(\mathcal{R}_1)\omega^{(2)}_j(\mathcal{R}_2) - \overrightarrow{\omega}^{(1)}_i(\mathcal{R}_1)\overrightarrow{\omega}^{(2)}_j(\mathcal{R}_2)\\
&\quad - \omega^{(12)}_{ij}(\mathcal{R}_1,\mathcal{R}_2)
\end{aligned} \tag{42}$$

of the mixed weight function from Eq. (38). The information about orientational anisotropy for the homogeneous fluid is then solely contained in the mixed weight function

$$\omega^{(12)}_{ij}(\mathcal{R}_1,\mathcal{R}_2) = \frac{\Delta\kappa}{4\pi}\frac{\left(\mathbf{v}^{I}_i\mathbf{n}_j\right)^2 - \left(\mathbf{v}^{II}_i\mathbf{n}_j\right)^2}{(1+\mathbf{n}_i\mathbf{n}_j)}\omega^{(2)}_i\omega^{(2)}_j, \tag{43}$$

which vanishes for a spherical shape like the tensorial weight function $\overleftrightarrow{\omega}^{(1)}_i$ from Eq. (25). The expressions which result from the second term on the right-hand side of Eq. (41) factorize to scalar and vectorial weight functions defined in Eqs. (9) and (10) as in edFMT [46].

Expanding of the denominator in Eq. (43), we find the series representation

$$\omega^{(12)}_{ij} = \sum_{r=2}^{\infty}\omega^{(12)}_{ij,[r]}. \tag{44}$$

We may factorize the mixed weight functions

$$\begin{aligned}
&\omega^{(12)}_{ij,[r]}(\mathcal{R}_1,\mathcal{R}_2)\\
&\quad = \frac{\Delta\kappa}{4\pi}\left[\left(\mathbf{v}^{I}_i\mathbf{n}_j\right)^2 - \left(\mathbf{v}^{II}_i\mathbf{n}_j\right)^2\right](-\mathbf{n}_i\mathbf{n}_j)^{r-2}\omega^{(2)}_i\omega^{(2)}_j
\end{aligned} \tag{45}$$

into tensorial weight functions of rank $r \geqslant 2$. In particular, we find the well-known representation

$$\omega^{(12)}_{ij,[2]} = \text{Tr}\left[\overleftrightarrow{\omega}^{(1)}_i\overleftrightarrow{\omega}^{(2)}_j\right] \tag{46}$$

of the first-order term with the rank-2 tensors defined in Eq. (25). Both of these equivalent approaches do have their advantages and drawbacks. Our new expansion from Eq. (44) in terms of mixed weight functions simplifies an analytic evaluation, as we do not have to consider single tensorial

components, which leads to a rapidly increasing number of terms.

D. Excess free energy

In Sec. II C, we found different representations for the mixed weight function $\Omega_{ij}^{(12)}$. The definition of the convolution from Eq. (37) applies to all mixed weight functions $\Omega_{ij,(\upsilon)}^{(12)} \in \{\Omega_{ij}^{(12)},\omega_{ij}^{(12)},\omega_{ij,[r]}^{(12)}\}$ found in alternative decompositions to Eq. (39), where υ is an arbitrary label. In analogy to the one-body weighted densities from Eq. (8), we define the corresponding mixed weighted densities $N_{12}^{(\upsilon)} \in \{N_{12},n_{12},n_{12}^{[r]}\}$ by

$$N_{12}^{(\upsilon)}(\mathbf{r}) = \sum_{i,j=1}^{\kappa} \iint d\mathcal{R}_1 d\mathcal{R}_2 \rho_i(\mathcal{R}_1)\rho_j(\mathcal{R}_2) \times \Omega_{ij,(\upsilon)}^{(12)}(\mathbf{r}-\mathcal{R}_1,\mathbf{r}-\mathcal{R}_2). \tag{47}$$

With the decomposition of the Mayer f function from Eq. (39), we obtain the low-density expression

$$\Phi_{\text{ex}}(\mathbf{r}) = n_0(\mathbf{r})n_3(\mathbf{r}) + N_{12}(\mathbf{r}) + \mathcal{O}(\rho^3), \tag{48}$$

of the excess free energy density corresponding to Eq. (27). This result gives rise to the exact second-virial coefficient and excluded volume in a fluid of anisotropic particles.

Note that Eq. (27) depends on the geometry of the body traced out by two overlapping particles via the Mayer bond. In contrast, Eq. (48), which becomes equal to Eq. (27) after integration over $\mathbf{r}$, depends only on single-particle properties, where the mixed weight function from Eq. (38) depends on the properties of two particles simultaneously. Solving a differential equation based on scaled-particle theory [67], we obtain the general excess free energy density

$$\Phi_{\text{ex}} = -n_0\ln(1-n_3) + \frac{\phi_2}{(1-n_3)} + \frac{\phi_3}{(1-n_3)^2} \tag{49}$$

at nonzero density. Alternatively, we find the structure of Eq. (49) from zero-dimensional cavities [48,57,58] or the virial expansion [68,69]. All these equivalent approaches for the extrapolation to finite density require the form of the low-density expression given by Eq. (48) and cannot be performed using Eq. (27) directly. We may replace $\phi_2 = N_{12}$ from the exact low-density limit in Eq. (48) with any equivalent or approximate form. In the third term, which is only relevant at nonzero density, there are different possibilities to choose $\phi_3(n_2,\overrightarrow{n}_2,\overleftrightarrow{n}_2)$.

According to Eq. (42), we can split the mixed weighted density

$$N_{12} = n_1n_2 - \overrightarrow{n}_1\overrightarrow{n}_2 - n_{12} =: \phi_2^{(\text{MM})} \tag{50}$$

into the four familiar one-body weighted densities [39] and the two-body measure n_{12}, which we additionally require to describe anisotropic systems [59]. With the expansion of $\omega_{ij}^{(12)}$ from Eq. (44), we define the approximate second term,

$$N_{12} \approx n_1n_2 - \overrightarrow{n}_1\overrightarrow{n}_2 - \sum_{r=2}^{r_{\text{t}}} n_{12}^{[r]} =: \phi_2^{[r_{\text{t}}]}, \tag{51}$$

for truncation at order $r = r_{\text{t}}$. For a homogeneous density, we only need to include weighted densities of even order $r = 2n$. Therefore, we can use a systematic expansion of n_{12} [51], which yields the approximate series representation

$$N_{12} \approx n_1n_2 - \sum_{n=1}^{n_{\text{t}}}\sum_{m=1}^{n} \zeta_m^{[n]} n_{12}^{[2m]} =: \phi_2^{\{\zeta^{[n_{\text{t}}]}\}}, \tag{52}$$

truncated at $n = n_{\text{t}}$. The parameters

$$\zeta_m^{[n]} = \frac{(-1)^{n+m}4^{-n}(4n+1)(2n+2m)!}{2n(n+1)(4n^2-1)(n+m)!(n-m)!(2m-2)!} \tag{53}$$

correct each term, such that Eq. (52) results in a series of order parameters, i.e., averaged Legendre polynomials, for the nematic phase. Originally, the correction $\zeta_1^{[1]} = 5/4$ for truncation at $n_{\text{t}} = 1$ was replaced by a free parameter ζ in edFMT [46]. According to Eq. (46), we can rewrite the second term

$$N_{12} \approx n_1n_2 - \overrightarrow{n}_1\overrightarrow{n}_2 - \zeta\,\text{Tr}[\overleftrightarrow{n}_1\overleftrightarrow{n}_2] =: \phi_2^{(\zeta)}, \tag{54}$$

using the tensorial weighted densities from Eq. (25).

The third term in Eq. (49) is vital for the description of anisotropic particles at finite packing [51]. A necessary criterion for an accurate expression, the correct crossover to low spatial dimensions [55,56], is fulfilled by both

$$\phi_3^{(\text{TR})}(n_2,\overleftrightarrow{n}_2) = \frac{3}{16\pi}\left(n_2^3 - 3n_2\text{Tr}\left[\overleftrightarrow{n}_2^2\right] + 2\text{Tr}\left[\overleftrightarrow{n}_2^3\right]\right) \tag{55}$$

and

$$\phi_3^{(\text{T})}(n_2,\overrightarrow{n}_2,\overleftrightarrow{n}_2) = \frac{3}{16\pi}\left(\overrightarrow{n}_2^{\,T}\overleftrightarrow{n}_2\overrightarrow{n}_2 - n_2\overrightarrow{n}_2\overrightarrow{n}_2 - \text{Tr}\left[\overleftrightarrow{n}_2^3\right] + n_2\text{Tr}\left[\overleftrightarrow{n}_2^2\right]\right), \tag{56}$$

derived by Tarazona and Rosenfeld [57] and Tarazona [58], respectively. It has been shown [51] that Tarazona's expression leads to a diverging free energy per particle for infinitely long rods and infinitely thin platelets. This deficiency makes it inappropriate for general fluids of anisotropic bodies, despite its consistency with Percus-Yevick theory [40].

Given any valid fundamental measure functional, i.e., an excess free energy which is written as a function of different weighted densities, it is straightforward to calculate an appropriate direct correlation function (DCF) without additional empirical input. Within DFT, the DCF

$$c_{ij}^{(2)}(\mathbf{r}=\mathbf{r}_1-\mathbf{r}_2,\mathbf{O}_1,\mathbf{O}_2) = -\frac{\delta^2\beta\mathcal{F}_{\text{ex}}[\{\rho_i(\mathcal{R}')\}]}{\delta\rho_i(\mathcal{R}_1)\delta\rho_j(\mathcal{R}_2)} \tag{57}$$

is conveniently defined as the second functional derivative of the free energy. Ordinary weighted densities are linear in the density. Therefore, their first functional derivative is equivalent to the corresponding weight functions and their second variation vanishes. We find the first functional derivative,

$$\frac{\delta N_{12}^{(\upsilon)}(\mathbf{r}')}{\delta\rho_k(\mathcal{R}_1)} = \sum_{j=0}^{\kappa}\int d\mathcal{R}_2'\rho(\mathcal{R}_2')\Omega_{kj,(\upsilon)}^{(12)}(\mathbf{r}'-\mathcal{R}_1,\mathbf{r}'-\mathcal{R}_2') + \sum_{i=0}^{\kappa}\int d\mathcal{R}_1'\rho(\mathcal{R}_1')\Omega_{ik,(\upsilon)}^{(12)}(\mathbf{r}'-\mathcal{R}_1',\mathbf{r}'-\mathcal{R}_1), \tag{58}$$

of a mixed weighted density. We can express the integral

$$\int d\mathbf{r}' \frac{\delta^2 N_{12}^{(\upsilon)}(\mathbf{r}')}{\delta\rho_i(\mathcal{R}_1)\delta\rho_j(\mathcal{R}_2)} = \Omega_{ij,(\upsilon)}^{(1\otimes 2)} + \Omega_{ji,(\upsilon)}^{(1\otimes 2)} \tag{59}$$

over the second functional derivative in terms of the self-convolution products defined in Eq. (37). The resulting DCF of FMMT reads

$$\begin{aligned} c_{ij}^{(2)}(\mathbf{r},\mathbf{O}_1,\mathbf{O}_2) = &- \sum_{\mu,\nu} \frac{\partial^2\Phi_{\mathrm{ex}}}{\partial n_\mu \partial n_\nu} \omega_i^{(\mu)} \otimes \omega_j^{(\nu)} - \sum_{\upsilon} \frac{\partial^2\Phi_{\mathrm{ex}}}{\partial n_3 \partial N_{12}^{(\upsilon)}} \\ &\times \left(\omega_i^{(3)} \otimes \frac{\delta N_{12}^{(\upsilon)}}{\delta\rho_j} + \frac{\delta N_{12}^{(\upsilon)}}{\delta\rho_i} \otimes \omega_j^{(3)} \right) \\ &- \sum_{\upsilon} \frac{\partial\Phi_{\mathrm{ex}}}{\partial N_{12}^{(\upsilon)}} \left(\Omega_{ij,(\upsilon)}^{(1\otimes 2)} + \Omega_{ji,(\upsilon)}^{(1\otimes 2)} \right) \end{aligned} \tag{60}$$

in its most general form. The summation over υ includes all involved mixed weights, whereas ν and μ account for scalar, vectorial, and tensorial one-body quantities.

III. FRANK ELASTIC COEFFICIENTS

We use the different versions of FMT derived in Sec. II to study the nematic phase of monodisperse hard spherocylinders. We calculate the corresponding orientational distributions analytically from a free minimization and compare the nematic equation of state in Sec. III A. In Sec. III B, we introduce the general approach to calculate the Frank elastic coefficients within FMT. We provide an approximate analytic solution in Sec. III C, which we evaluate in Sec. III D for low-ordered systems and the Onsager limit. We discuss the behavior of the elastic coefficients as a function of the density and the nematic order parameter in Sec. III E, comparing the full result of FMMT to the analytic series representation and other works.

A. Nematic orientational distribution

The uniaxial nematic bulk phase of monodisperse hard spherocylinders has a translational symmetry in the direction $\hat{n}$ of the nematic director, in which the particles preferably align. Therefore, the dependence on the orientation $\mathbf{O}$ reduces to $\varpi = (\theta,\phi)$, such that the orientational average becomes

$$\int d\mathbf{O} = \int d\varpi = \frac{1}{2\pi} \int_0^{2\pi} d\phi \int_0^1 d\cos\theta. \tag{61}$$

We choose the z direction for the nematic director. The particle orientation

$$\hat{\varpi} = \begin{pmatrix} \cos\phi \sin\theta \\ \sin\phi \sin\theta \\ \cos\theta \end{pmatrix} \tag{62}$$

corresponds to the radial unit vector in spherical coordinates. Then the distribution $g(\hat{n}\hat{\varpi}) = g(\cos\theta)$ of orientations takes its most simple form only depending on the cosine of the azimuthal angle θ [49]. The explicit function follows from the variation according to Eq. (26) with a homogeneous density $\rho(\mathbf{r}) \equiv \rho$. To this end, it is desirable to use an analytic representation of the excess free energy density Φ_{ex} in Eq. (49). The easiest way to do so is the common ζ correction from Eq. (54) with the well-known one-body weighted densities [47,49],

$$\begin{aligned} n_3 &= \rho\left(\frac{\pi}{4}LD^2 + \frac{\pi}{6}D^3\right) = \rho v = \eta, \\ n_2 &= \rho(\pi LD + \pi D^2), \\ n_1 &= \rho\left(\frac{L}{4} + \frac{D}{2}\right), \quad n_0 = \rho, \\ (\overleftrightarrow{n}_2)_{11} &= (\overleftrightarrow{n}_2)_{22} = \rho\left[\frac{\pi}{6}LD(2+S) + \frac{\pi}{3}D^2\right], \\ (\overleftrightarrow{n}_2)_{33} &= \rho\left[\frac{\pi}{3}LD(1-S) + \frac{\pi}{3}D^2\right], \\ (\overleftrightarrow{n}_1)_{11} &= (\overleftrightarrow{n}_1)_{22} = -\frac{1}{2}(\overleftrightarrow{n}_1)_{33} = \rho\frac{L}{8}S, \end{aligned} \tag{63}$$

of spherocylinders with diameter D, cylinder length L, volume v, and aspect ratio $l = L/D$. The orientation dependence is contained in the nematic order parameter

$$S = \int_0^1 d\cos\theta \left(\frac{3}{2}\cos\theta^2 - \frac{1}{2}\right) g(\cos\theta), \tag{64}$$

where we simplified the orientational average from Eq. (61) according to the symmetry of $g(\cos\theta)$ and η denotes the packing fraction.

For the mixed weighted densities of order $2m$, we find

$$\sum_{m=1}^{n} \zeta_m^{[n]} n_{12}^{[2m]} = \rho^2 L^2 D\pi \frac{(4n+1)(2n-3)!!(2n-1)!!}{2^{2n+2}n!(n+1)!} \bar{P}_{2n}^2 \tag{65}$$

with the prefactors from Eq. (53). Hence, the expansion from Eq. (52) gives rise to a sequence of n_{t} order parameters,

$$\bar{P}_{2n} := \int_0^1 d\cos\theta\, P_{2n}(\cos\theta) g(\cos\theta), \tag{66}$$

which are orientationally averaged Legendre polynomials $P_{2n}(x)$, where $S \equiv \bar{P}_2$ [51]. We find a closed expression $g(\{P_{2n}(\cos\theta)\})$ for the orientational distribution from the variation of the corresponding excess free energy. The minimization requires solving the n_{t} equations for the intrinsic order parameters $\alpha_{[2n]}^2 := -\partial\Phi_{\mathrm{ex}}/\partial\bar{P}_{2n}/\rho$ plus the numerical normalization of the distribution [51]. For $n_{\mathrm{t}} = 1$, we obtain the normalized distribution

$$g(\alpha,\cos\theta) = \frac{\alpha}{\mathcal{D}(\alpha)} \exp[-\alpha^2(1-\cos^2\theta)] \tag{67}$$

in terms of Dawson's integral $\mathcal{D}(\alpha)$ and the intrinsic order parameter $\alpha^2 = 3\alpha_{[2]}^2/2$ [47].

The quick convergence of Eq. (52) when increasing n_{t} at isotropic-nematic coexistence has already been demonstrated in Ref. [51]. However, the minimization beyond $n_{\mathrm{t}} = 10$ becomes increasingly difficult. We therefore impose Eq. (67) as the orientational distribution for the remainder of this work. Then we find the recurrence formulas

$$I_{2n} = \frac{1}{2\alpha\mathcal{D}(\alpha)} - \frac{(2n-1)I_{2n-2}}{2\alpha^2}, \quad I_2 = \frac{\alpha - \mathcal{D}(\alpha)}{2\alpha^2\mathcal{D}(\alpha)} \tag{68}$$

TABLE I. Test of the generalized ζ correction from Eq. (52) with different truncation orders $2n_t$ as an approximation for the mixed weighted density n_{12}. We minimize the functionals for different packing fractions η of hard spherocylinders with aspect ratio $l = 20$. The third term is from Eq. (55). We show the approximate results $\tilde{n}_{12}$ for the truncated expansion of n_{12} imposing the orientational distribution from Eq. (67) and calculate the difference $\Delta\tilde{n}_{12}$ subtracting the result of a free minimization for the same n_t, where e-x is short for $\times 10^{-x}$. Missing values denote that we were unable to perform the free minimization due to the high computational effort for $n_t > 10$. At first order $n_t = 1$, the free minimization is equivalent to our approximation. We also show the result for the nematic order parameter S and pressure p. The largest value of n_t denotes the lowest-order term whose addition changes βpv by less than 10^{-6}. Then the expansion has certainly converged. Imposing the respective order parameter, we confirm this result evaluating the full mixed weighted density n_{12}, denoted by $n_t = \infty$. The number in brackets denotes the error in the last digit due to four-dimensional (see text) Monte Carlo integration with 10^7 function calls taking about 40 s.

η	n_t	$\tilde{n}_{12}D^3$	$\Delta\tilde{n}_{12}D^3$	S	βpv
0.3	1	0.057 90	0	0.9291	3.162
0.3	2	0.071 41	3.2e-6	0.9508	2.623
0.3	3	0.077 23	1.3e-5	0.9602	2.390
0.3	5	0.082 10	4.2e-5	0.9686	2.191
0.3	8	0.084 18	4.0e-5	0.9725	2.106
0.3	10	0.084 48	−1.8e-5	0.9731	2.093
0.3	19	0.084 56		0.9733	2.090
0.3	∞	0.084 57(2)		0.9733	2.090
0.5	1	0.179 17	0	0.9806	15.83
0.5	2	0.218 94	5.5e-8	0.9854	12.98
0.5	3	0.236 59	4.6e-7	0.9881	11.68
0.5	5	0.252 82	3.3e-6	0.9910	10.46
0.5	8	0.262 65	1.5e-5	0.9930	9.704
0.5	10	0.265 89	2.7e-5	0.9938	9.451
0.5	20	0.271 04		0.9951	9.043
0.5	44	0.271 41		0.9953	9.007
0.5	∞	0.271 41(2)		0.9953	9.007

for the moments

$$I_r = \int_0^1 d\cos\theta \cos^r\theta g(\cos\theta), \tag{69}$$

which are zero for odd values of r. The order parameters from Eq. (66) have the explicit form

$$\bar{P}_{2n} = \sum_{k=0}^{n}(-1)^k \frac{(4n-2k)!}{4^n(2n-k)!(2n-2k)!k!} I_{2n-2k}. \tag{70}$$

Therefore, the equilibrium condition

$$\frac{\partial\Phi}{\partial\alpha} = 0, \tag{71}$$

with respect to the orientational degrees of freedom, exclusively involves the intrinsic order parameter α. The effort for solving this self-consistency equation for an arbitrary truncation order is practically the same as a free minimization for $n_t = 1$.

In Table I, we see that the difference between the Gaussian approximation, Eq. (67), for the nematic orientational distribution and a full minimization is negligible. At $n_t = 10$, the error due to truncation is still larger, which we see adding higher-order terms. Particularly at high packing fractions η, far beyond the isotropic-nematic coexistence region, we may not consider the truncated expansion with $n_t = 10$ as converged. To further illustrate the convergence, we consider the equation of state $p(\eta)$ for different n_t in Fig. 2. For the third term in the free energy, we use $\phi_3^{(TR)}$ from Eq. (55), which results in a good agreement with computer simulations [70]. The original approach with Eq. (56) significantly overestimates the nematic pressure [51], although the parameter $\zeta = 1.6$ in Eq. (54) was chosen to fit the densities at the isotropic-nematic coexistence to the result from Ref. [71]. The isotropic branch does not depend on the order of truncation, as $n_{12} = 0$ in the isotropic phase and only the lowest nematic order parameter S determines the limit of metastability with respect to a nematic perturbation. The nematic pressure decreases with increasing number of terms and has converged at least at $n_t = 50$. In comparison, we see that the difference between this full solution and the result at small n_t increases with the density. The approximation by rank-2 tensors from Eq. (54), which is equivalent to $n_t = 1$, is not sufficient for the nematic phase.

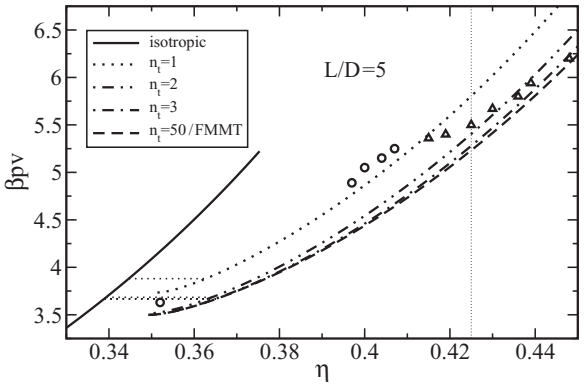

FIG. 2. Isotropic (solid line) and nematic equations of state of hard spherocylinders with aspect ratio $l = 5$. We use the generalized ζ correction from Eq. (52) with different truncation orders n_t and the expression $\phi_3^{(TR)}$ from Eq. (55) by Tarazona and Rosenfeld. The convergence of this expansion towards the FMMT result with the full mixed weighted density, Eq. (50), becomes slower with increasing packing fraction η and nematic order parameter. The horizontal dotted lines indicate the isotropic-nematic coexistence pressure and densities. The vertical dotted line denotes the limit of stability with respect to the smectic-A phase obtained with FMMT [59]. The circles and triangles denote the simulation results [70] for the isotropic and nematic branch, respectively.

We have seen that the simple orientational distribution from Eq. (67), together with the systematic calculation of higher-order terms, provides a simple but reliable description of the nematic bulk phase. This Gaussian approximation was also used for the mixed weighted densities n_{12} and N_{12} to study the isotropic-nematic interface and the smectic-A phase numerically [59]. For the nematic bulk phase, a numerical calculation requires the four integrations over z_1, z_2, φ_1, and φ_2 in cylindrical coordinates of the two spherocylinders. Beforehand, we perform the integrals over the polar orientational

angles ϕ_1 and ϕ_2 analytically and only add the two numerical averages with respect to θ_1 and θ_2. Evaluating n_{12} instead of N_{12}, the integrals over z_1 and z_2 become trivial as the hemispherical contributions vanish. Therefore, we perform a four-dimensional Monte Carlo integration. However, we cannot solve Eq. (71) to determine the order parameter α analytically. Therefore, we use the approximation in Eq. (52) with the sufficiently large truncation order $n_t = 50$ to calculate the corresponding value of α. Doing so, we verify in Table I that the mixed weighted density n_{12} is indeed the limit of this convenient expansion. We may use both approaches interchangeably and therefore identify the nematic branch in Fig. 2 corresponding to $n_t = 50$ with the full FMMT result. Note that in systems of parallel bodies, we can calculate the mixed weighted densities of hard spherocylinders explicitly [59] and verify the agreement with the series representation [51] directly. Now we are prepared to calculate the Frank elastic coefficients with both FMMT and different expansions.

B. Poniewierski-Stecki equations

External potentials break the symmetry of the nematic bulk fluid. Surfaces imposing a particular orientation of the nematic director or aligning fields that act on the orientation ϖ induce elastic deformations. The continuum description in Eq. (1) due to Frank does not account for microscopic details, such as the spatial density distribution or the molecular shape. Microscopically, the nematic director field is contained implicitly in the inhomogeneous orientational distribution as the direction in which it attains its maximum for a fixed position. In equilibrium, we assume the form of Eq. (67) with a director field $\hat{n} = (0,0,1)$ parallel to the z axis.

We describe the elasticity of the nematic phase using the variational DFT approach [17] from Eq. (2). These Poniewierski-Stecki equations require an appropriate DCF which we can provide for all FMT functionals according to Eq. (60). We obtain the orientational component $\hat{\varpi}_x = \cos\phi\sin\theta$ and the derivative $\rho'(\hat{n}\cdot\hat{\varpi}) = \rho g'(\cos\theta)$ of the orientation-dependent density from the unit vector in Eq. (62). With the analytic orientational distribution from Eq. (67), we calculate

$$g'(\alpha,\cos\theta) = \frac{dg(\alpha,\cos\theta)}{\mathrm{d}\cos\theta} = g(\alpha,\cos\theta)2\alpha^2\cos\theta. \quad (72)$$

Separating the spatial integral

$$R_\epsilon(\varpi,\varpi') := -\int d\mathbf{r} r_\epsilon^2 c^{(2)}(\mathbf{r},\varpi,\varpi') \quad (73)$$

from the universal orientational part

$$W(\alpha,\varpi) := g(\alpha,\cos\theta)2\alpha^2\cos\theta\hat{\varpi}_x(\theta,\phi), \quad (74)$$

we rewrite Eq. (2) as

$$\beta K_\epsilon = -\frac{\rho^2}{2}\iint d\varpi d\varpi' R_\epsilon(\varpi,\varpi')W(\alpha,\varpi)W(\alpha,\varpi'). \quad (75)$$

To calculate the spatial integral in Eq. (73), we parametrize the spherocylinder in body-fixed cylindrical coordinates $\bar{\mathbf{r}} = (\bar{z},\bar{\varrho},\bar{\varphi})$ and include the orientation-dependence implicitly in the weight functions, as described in Ref. [49]. Within the space-fixed outer coordinate frame, the position vector $\mathbf{r}(\bar{\mathbf{r}},\varpi)$ reads

$$\mathbf{r} = \begin{pmatrix} \cos\phi\cos\theta\bar{\varrho}\cos\bar{\varphi} - \sin\phi\bar{\varrho}\sin\bar{\varphi} + \cos\phi\sin\theta\bar{z} \\ \sin\phi\cos\theta\bar{\varrho}\cos\bar{\varphi} + \cos\phi\bar{\varrho}\sin\bar{\varphi} + \sin\phi\sin\theta\bar{z} \\ -\sin\theta\bar{\varrho}\cos\bar{\varphi} + \cos\theta\bar{z} \end{pmatrix}. \quad (76)$$

The volume element becomes $d\mathbf{r} = d\bar{\mathbf{r}} = \bar{\varrho}d\bar{\varrho}d\bar{\varphi}d\bar{z}$.

Now that we have introduced all ingredients to Eq. (2), we insert the general form of the DCF from Eq. (60) into the integrand in Eq. (73). To this end, we consider the functional

$$T_\epsilon[\mathfrak{H}](\varpi,\varpi') := \int d\mathbf{r} r_\epsilon^2 \mathfrak{H}(\mathbf{r},\varpi,\varpi') \quad (77)$$

of an arbitrary function $\mathfrak{H}(\mathbf{r},\varpi,\varpi')$. Including the orientational averages, we define

$$\mathcal{T}_\epsilon[\mathfrak{H}] := \iint d\varpi d\varpi' T_\epsilon[\mathfrak{H}](\varpi,\varpi')W(\alpha,\varpi)W(\alpha,\varpi'). \quad (78)$$

Applying this functional to the convolution product $\omega^{(\nu)}\otimes\omega^{(\mu)}$ of two weight functions and the self-convolution $\Omega_{(\upsilon)}^{(1\otimes 2)}$, we find Eq. (3) from Eq. (75).

For any convolution, we can simplify the integrals within

$$\begin{aligned} T_\epsilon[\omega^{(\nu)}\otimes\omega^{(\mu)}] &= \int d\mathbf{r} r_\epsilon^2 \omega^{(\nu)}\otimes\omega^{(\mu)}(\mathbf{r},\varpi,\varpi') \\ &= \iint d\mathbf{r} d\mathbf{r}' r_\epsilon^2 \omega^{(\nu)}(\mathbf{r}'-\mathbf{r},\varpi)\omega^{(\mu)}(\mathbf{r}',\varpi') \\ &= \iint d\mathbf{r}' d\mathbf{r} (r_\epsilon'-r_\epsilon)^2 \omega^{(\nu)}(\mathbf{r},\varpi)\omega^{(\mu)}(\mathbf{r}',\varpi') \end{aligned} \quad (79)$$

by substituting $\mathbf{r}\to\mathbf{r}'-\mathbf{r}$. With these two similar integrals, we can simplify the first term in Eq. (3), which does not contain mixed weight functions. The expression

$$\mathcal{T}_\epsilon[\omega^{(\nu)}\otimes\omega^{(\mu)}] = \bar{\omega}_{(\epsilon,2)}^{(\nu)}\bar{\omega}_{(\epsilon,0)}^{(\mu)} - 2\bar{\omega}_{(\epsilon,1)}^{(\nu)}\bar{\omega}_{(\epsilon,1)}^{(\mu)} + \bar{\omega}_{(\epsilon,0)}^{(\nu)}\bar{\omega}_{(\epsilon,2)}^{(\mu)}, \quad (80)$$

only contains the integrals

$$\bar{\omega}_{(\epsilon,q)}^{(\nu)} = \int d\mathcal{R} r_\epsilon^q \omega^{(\nu)}(\mathcal{R})W(\alpha,\varpi),\ q\in\{0,1,2\} \quad (81)$$

over the weight functions of one body. We can further show that the second term in Eq. (60), involving the first functional derivative of mixed weighted densities, does not contribute to Eq. (3), as $\bar{\omega}_{(\epsilon,q)}^{(3)} = 0$ for all q in the uniaxial nematic phase. Now we define the different contributions to the elastic coefficients which correspond to the different versions of the second ϕ_2 and third terms ϕ_3 of the functional, Eq. (49), introduced in Sec. II D.

As a first step, we consider the excess free energy in the first-order approximation for the mixed weighted density, setting $r_t = 2$ in Eq. (51) and use the one-body weighted densities of a spherocylinder from Eq. (63). For a cylindrical symmetric body, we have $\bar{\omega}_{(\epsilon,1)}^{(\nu)} = 0$ for all weight functions and find $\bar{\omega}_{(\epsilon,0)}^{(\nu)} \neq 0$ only for the off-diagonal tensorial components $(\overleftrightarrow{\omega}^{(1)})_{13}$ and $(\overleftrightarrow{\omega}^{(2)})_{13}$. Hence, there are only two

contributions to the first sum in Eq. (3), which respectively arise from ϕ_2 and ϕ_3. We accordingly define the leading term

$$\beta K_{\epsilon,2}^{[2]} := \frac{2\rho^2}{1-n_3}\mathcal{T}_\epsilon[(\overleftrightarrow{\omega}^{(1)})_{13}\otimes(\overleftrightarrow{\omega}^{(2)})_{13}], \tag{82}$$

corresponding to the expansion of ϕ_2 and the two possible contributions

$$\beta K_{\epsilon,3}^{(\mathrm{TR})} := \frac{9\rho^2[-(\overleftrightarrow{n}^{2})_{22}-(\overleftrightarrow{n}^{2})_{33}+n_2]}{8\pi(1-n_3)^2} \times \mathcal{T}_\epsilon[(\overleftrightarrow{\omega}^{(2)})_{13}\otimes(\overleftrightarrow{\omega}^{(2)})_{13}] \tag{83}$$

and

$$\beta K_{\epsilon,3}^{(\mathrm{T})} := \frac{\rho^2[3(\overleftrightarrow{n}^{2})_{22}+3(\overleftrightarrow{n}^{2})_{33}-2n_2]}{16\pi(1-n_3)^2} \times \mathcal{T}_\epsilon[(\overleftrightarrow{\omega}^{(2)})_{13}\otimes(\overleftrightarrow{\omega}^{(2)})_{13}] \tag{84}$$

of the third terms from Eq. (55) or Eq. (56), respectively.

Using mixed measures instead, we can easily calculate the higher-order terms

$$K_{\epsilon,2}^{[r]} = \frac{\rho^2}{1-n_3}\mathcal{T}_\epsilon\big[\omega_{[r]}^{(1\otimes 2)}\big], \tag{85}$$

recovering the result of Eq. (82) for $r=2$. The exact contribution

$$\beta K_{\epsilon,2}^{(\mathrm{MM})} = -\frac{\rho^2}{1-n_3}\mathcal{T}_\epsilon[\Omega^{(1\otimes 2)}] = \frac{\rho^2}{1-n_3}\mathcal{T}_\epsilon[\omega^{(1\otimes 2)}] \tag{86}$$

of the second term in Eq. (49) to the elastic coefficients only involves the second functional derivative of either mixed weighted density N_{12} or n_{12}, as the scalars and vectors do not contribute to $\mathcal{T}_\epsilon$.

C. Analytic Frank constants of spherocylinders

Now we explicitly calculate analytic formulas for the Frank elastic coefficients in the nematic phase of hard spherocylinders. In the integrand of Eq. (78), we find polynomials in $\cos\theta$ and $\cos\theta'$ of degree at least $r+4$, where r is the order (rank) of the corresponding mixed (tensorial) weight function. Therefore, we easily find a representation in terms of the orientational moments I_{2n} from Eq. (69). We begin by calculating the individual contributions defined in Sec. III B.

From either Eq. (82) or Eq. (85), we obtain the first-order results for the contribution from the second term,

$$\begin{aligned}
\beta K_{1,2}^{[2]} &= \frac{C_N[(I_2+2I_4-3I_6)+3l^2(I_2-2I_4+I_6)]}{64(1-\eta)},\\
\beta K_{2,2}^{[2]} &= \frac{C_N[(4I_2-3I_4-I_6)+l^2(I_2-2I_4+I_6)]}{64(1-\eta)},\\
\beta K_{3,2}^{[2]} &= \frac{C_N[(I_2-2I_4+I_6)+l^2(I_4-I_6)]}{16(1-\eta)},
\end{aligned} \tag{87}$$

with the common factor

$$C_N := \rho^2L^2D^3\alpha^4\pi(I_2-I_4). \tag{88}$$

We introduce the superscript $(\cdot)$, which stands for (TR) or (T) denoting the choice for the third term from Eq. (83) or Eq. (84), respectively. The contribution from the third term reads

$$\begin{aligned}
\beta K_{1,3}^{(\cdot)} &= \frac{C_3^{(\cdot)}[3(I_2+2I_4-3I_6)+12l^2(I_2-2I_4+I_6)]}{2048(1-\eta)^2},\\
\beta K_{2,3}^{(\cdot)} &= \frac{C_3^{(\cdot)}[3(3I_2-2I_4-I_6)+4l^2(I_2-2I_4+I_6)]}{2048(1-\eta)^2},\\
\beta K_{3,3}^{(\cdot)} &= \frac{C_3^{(\cdot)}[3(I_2-2I_4+I_6)+4l^2(I_4-I_6)]}{512(1-\eta)^2},
\end{aligned} \tag{89}$$

where the different choices for the third term differ in the factors

$$C_3^{(\mathrm{TR})} = C_N\frac{\rho}{2}D^2[3L(I_2+1)+4D], \tag{90}$$

$$C_3^{(\mathrm{T})} = -C_N\frac{\rho}{4}LD^2(3I_2-1). \tag{91}$$

Our objective is to find a representation of the elastic coefficients solely in terms of the packing fraction η, the aspect ratio l, and the nematic order parameters $\bar{P}_{2n}$ from Eq. (66). To this end, we substitute the moments I_{2n} with their explicit expressions in terms of α and Dawson's integral $\mathcal{D}(\alpha)$ from Eq. (68). According to Eq. (70), we find a similar representation for the order parameters, which we now compare to Eq. (87). We obtain the desired expressions

$$\begin{aligned}
\beta K_{1,2}^{[2]}D &= \frac{9\eta^2l^2S[(4S+3\bar{P}_4)+3l^2(S-\bar{P}_4)]}{7\pi(1-\eta)(3l+2)^2},\\
\beta K_{2,2}^{[2]}D &= \frac{9\eta^2l^2S[(31S+4\bar{P}_4)+4l^2(S-\bar{P}_4)]}{28\pi(1-\eta)(3l+2)^2},\\
\beta K_{3,2}^{[2]}D &= \frac{9\eta^2l^2S[4(S-\bar{P}_4)+l^2(3S+4\bar{P}_4)]}{7\pi(1-\eta)(3l+2)^2},
\end{aligned} \tag{92}$$

for the Frank constants. The equilibrium order parameters follow from $\alpha(\eta,l)$ according to Eq. (71). Note that our analytical orientational distribution $g(\alpha,\cos\theta)$ from Eq. (67) is the key to understanding the nontrivial relation between Eqs. (87) and (92), which does not contain the factor α^4.

With the same procedure for Eq. (89), we find similar formulas for $K_{\epsilon,3}^{(\cdot)}$ from Eqs. (83) and (84). The results are shown in Appendix B. A significant difference between these results is the appearance of the additional order parameter $\bar{P}_6$ in $K_{\epsilon,3}^{(\mathrm{TR})}$ and the lack of a term proportional to S^2 in $K_{\epsilon,3}^{(\mathrm{T})}$, which is not apparent in Eqs. (90) and (91), respectively. We also provide the expressions $K_{\epsilon,2}^{[r]}$ from Eq. (85) up to order $r=7$ in Appendix B. Interestingly, only the terms $r_\epsilon^2+r_\epsilon'^2$ or $-2r_\epsilon r_\epsilon'$ in the integrand of Eq. (79) contribute to the elastic coefficients of even or odd order, respectively. The formulas for $K_{\epsilon,2}^{[2n]}$ and $K_{\epsilon,2}^{[2n+1]}$ depend on order parameters up to $\bar{P}_{2n+2}$. Note that the equilibrium values of $\bar{P}_{2n}$ depend on the truncation order n_t in Eq. (52). Therefore, we first need to determine the consistent nematic order parameters via Eq. (71) for each functional and then calculate the individual contributions to the elastic coefficients. We do not find an analytic representation of the elastic coefficients from Eq. (86), which are exact up to second order in density.

Finally, we collect these contributions to the expressions for the elastic coefficients. The full expressions for the elastic

coefficients of FMMT read

$$K_\epsilon^{(\mathrm{MM})} := K_{\epsilon,2}^{(\mathrm{MM})} + K_{\epsilon,3}^{(\cdot)}. \tag{93}$$

Introducing the ζ correction for truncation after the first term as in Eq. (54), we obtain the approximation

$$K_\epsilon^{(\mathrm{MM})} \approx \zeta K_{\epsilon,2}^{[2]} + K_{\epsilon,3}^{(\cdot)} =: K_\epsilon^{(\zeta)}. \tag{94}$$

We further consider the expansion

$$K_\epsilon^{(\mathrm{MM})} \approx \sum_{n=1}^{n_\mathrm{t}} \sum_{m=1}^{n} \zeta_m^{[n]} K_{\epsilon,2}^{[2m]} + \sum_{m=1}^{m_\mathrm{t}} K_{\epsilon,2}^{[2m+1]} + K_{\epsilon,3}^{(\cdot)} \tag{95}$$

using the generalized ζ correction for the even-order terms as in Eq. (52) and adding the odd-order terms up to $r = 2m_\mathrm{t} + 1$.

D. Extreme order parameters and Onsager limit

Now we use the analytic formulas, as found in Sec. III C and Appendix B, to examine certain limiting cases for the elastic coefficients. To determine the low-order behavior, we expand the order parameters

$$S = \frac{2}{15}\alpha^2 + \mathcal{O}(\alpha^4), \quad \bar{P}_4 = \frac{4}{315}\alpha^4 + \mathcal{O}(\alpha^6),$$
$$\bar{P}_6 = \frac{8}{9009}\alpha^6 + \mathcal{O}(\alpha^8), \quad \bar{P}_{2n} = \mathcal{O}(\alpha^{2n}), \tag{96}$$

in terms of α. Hence, the leading terms are proportional to $S^2 \propto \alpha^4$. In this limit, we find $K_1 = K_3$ for any approach. Within the ζ approximation, the elastic coefficients from Eq. (94) become

$$\beta K_1^{(\zeta)} D = \zeta \frac{9\eta^2 l^2 (4 + 3l^2)}{7\pi(1-\eta)(3l+2)^2} S^2 + \frac{81\eta^3 l^2 (l+1)(l^2+1)}{7\pi(1-\eta)^2(3l+2)^3} S^2 + \mathcal{O}(\alpha^6),$$
$$\beta K_2^{(\zeta)} D = \zeta \frac{9\eta^2 l^2 (31 + 4l^2)}{28\pi(1-\eta)(3l+2)^2} S^2 + \frac{27\eta^3 l^2 (l+1)(2l^2+9)}{14\pi(1-\eta)^2(3l+2)^3} S^2 + \mathcal{O}(\alpha^6), \tag{97}$$

when using $\phi_3^{(\mathrm{TR})}$. The respective formulas for $\phi_3^{(\mathrm{T})}$ only contain the term proportional to the ζ parameter.

As an application, we used Eq. (97) in an earlier paper [49] to determine the parameters L_1 and L_2 in the elastic free energy [14]

$$f_d = \frac{\beta}{2}(L_1 Q_{\alpha\beta,\gamma} Q_{\alpha\beta,\gamma} + L_2 Q_{\alpha\gamma,\alpha} Q_{\beta\gamma,\beta}) + \mathcal{O}[(\nabla Q)^3] \tag{98}$$

of Landau-de Gennes theory for hard spherocylinders. The abbreviation $Q_{\alpha\beta,\gamma} := \partial_\gamma Q_{\alpha\beta}$ denotes the partial derivative $\partial_\gamma = \partial/\partial r_\gamma$ of the order tensor

$$Q_{\alpha\beta}(\mathbf{r}) = Q(\mathbf{r})\left[\hat{n}_\alpha(\mathbf{r})\hat{n}_\beta(\mathbf{r}) - \tfrac{1}{3}\delta_{\alpha\beta}\right]. \tag{99}$$

The scalar order parameter $Q(\mathbf{r}) \equiv S$ in an elastically deformed nematic phase is uniform. Therefore, only derivatives of the director field $\hat{n}(\mathbf{r})$ are relevant and Eq. (98) simplifies to

$$f_d = \frac{\beta S^2}{2}[L_1 \partial_\gamma(\hat{n}_\alpha\hat{n}_\beta)\partial_\gamma(\hat{n}_\alpha\hat{n}_\beta) + L_2 \partial_\alpha(\hat{n}_\alpha\hat{n}_\gamma)\partial_\beta(\hat{n}_\beta\hat{n}_\gamma)]. \tag{100}$$

Comparing this expression with Eq. (1), we find [14]

$$K_1 = K_3 = S^2(2L_1 + L_2), \quad K_2 = 2S^2 L_1. \tag{101}$$

Substituting Eq. (97), we obtain the Landau parameters

$$\beta L_1^{(\zeta)} D = \zeta \frac{9\eta^2 l^2 (4l^2+31)}{56\pi(1-\eta)(3l+2)^2} + \frac{27\eta^3 l^2 (l+1)(2l^2+9)}{28\pi(1-\eta)^2(3l+2)^3},$$
$$\beta L_2^{(\zeta)} D = \zeta \frac{9\eta^2 l^2 (8l^2-15)}{28\pi(1-\eta)(3l+2)^2} + \frac{27\eta^3 l^2 (l+1)(4l^2-3)}{14\pi(1-\eta)^2(3l+2)^3}. \tag{102}$$

Note that in Ref. [49] we only considered the functional with $\phi_3^{(\mathrm{T})}$ from Eq. (56). Therefore, only the terms proportional to ζ in Eq. (102) are present therein. With the help of these elastic parameters and Landau-de Gennes theory, we find an analytic expression for the interfacial tension γ_{IN} between coexisting isotropic and nematic phases of hard spherocylinders [49].

Considering the low-order behavior, the relations

$$K_{\epsilon,2}^{[2n]} = \frac{15}{(2n+3)(2n+1)(2n-1)} K_{\epsilon,2}^{[2]} + \mathcal{O}(\alpha^6),$$
$$K_{\epsilon,2}^{[2n+1]} = \frac{105}{(2n+5)(2n+3)(2n+1)} K_{\epsilon,2}^{[3]} + \mathcal{O}(\alpha^6), \tag{103}$$

hold at least up to $n = 10$. While we were unable to prove this for general n, $K_{\epsilon,2}^{[r]}$ is already almost negligible at this order: $K_{\epsilon,2}^{[r]}/K_{\epsilon,2}^{[2]} \simeq 15/r^3 \simeq 2 \times 10^{-3}$ for $r = 2n = 20$ and $K_{\epsilon,2}^{[r]}/K_{\epsilon,2}^{[2]} \simeq (105/15)/r^3 \simeq 10^{-3}$ for $r = 2n + 1 = 21$. Therefore, we proceed to sum up both expressions from $n = 1$ to ∞ according to

$$K_{\epsilon,2}^{(\mathrm{MM})} = \sum_{r=2}^{\infty} K_{\epsilon,2}^{[r]} = \frac{5}{4} K_{\epsilon,2}^{[2]} + \frac{7}{4} K_{\epsilon,2}^{[3]} + \mathcal{O}(\alpha^6) \tag{104}$$

to find an analytic representation,

$$\beta K_{1,2}^{(\mathrm{MM})} D = \frac{135\eta^2 l^2 (l^2+2)}{28\pi(1-\eta)(3l+2)^2} S^2 + \mathcal{O}(\alpha^6),$$
$$\beta K_{2,2}^{(\mathrm{MM})} D = \frac{45\eta^2 l^2 (l^2+9)}{28\pi(1-\eta)(3l+2)^2} S^2 + \mathcal{O}(\alpha^6), \tag{105}$$

for Eq. (86) up to quadratic order in S. This result perfectly agrees with a numeric calculation of $K_{\epsilon,2}^{(\mathrm{MM})}$ for a small enough value of α. Neglecting the odd-order terms in Eq. (103) at large enough aspect ratio, we can account for the contributions in Eq. (105) approximately by a simple rescaling with $\zeta = 5/4$ in Eq. (97). This value has been found earlier to minimize the quadratic deviation to the exact excluded volume of hard spherocylinders [46] and coincides with the first coefficient $\zeta_1^{[1]} = 5/4$ of the systematic expansion from Eq. (53).

Now we discuss of the ratios $(K_\epsilon - \bar{K})/\bar{K}$ for our analytic representations of the Frank constants, where

$$\bar{K} = \tfrac{1}{3}(K_1 + K_2 + K_3). \tag{106}$$

Using the Onsager approximation, Priest discovered the fundamental expansion [13],

$$\frac{K_1-\bar{K}}{\bar{K}} = \Delta - 3\Delta'\frac{\bar{P}_4}{\bar{P}_2} + \cdots,$$
$$\frac{K_2-\bar{K}}{\bar{K}} = -2\Delta - \Delta'\frac{\bar{P}_4}{\bar{P}_2} + \cdots,$$
$$\frac{K_3-\bar{K}}{\bar{K}} = \Delta + 4\Delta'\frac{\bar{P}_4}{\bar{P}_2} + \cdots, \tag{107}$$

into ratios of order parameters. The prefactors Δ and Δ' are universal constants, which only depend on the particle shape. Hence, we find $K_1 \neq K_3$ beyond the low-order limit. Note that we can read Eq. (107) as an expansion up to the quadratic term in α.

First, we neglect the contributions of the third term ϕ_3 of the functional in Eq. (49) to the elastic coefficients. In that case, we easily see from Eq. (94) that the ratios of the elastic coefficients in the second-order approximation are independent of the ζ parameter. Explicitly, we find

$$\Delta_{[2]} = \frac{1}{7}\frac{8l^2-15}{4l^2+9}, \quad \Delta'_{[2]} = \frac{12}{7}\frac{l^2-1}{4l^2+9}, \tag{108}$$

from $K^{[2]}_{\epsilon,2}$.

Including higher-order terms $K^{[r]}_{\epsilon,2}$ up to $r = r_\mathrm{t}$, the constants $\Delta_{[r_\mathrm{t}]}$ and $\Delta'_{[r_\mathrm{t}]}$ vary nonmonotonously with the truncation order. It is not as straightforward as in Eq. (104) to determine $\Delta_{(\mathrm{MM})}$ and $\Delta'_{(\mathrm{MM})}$ corresponding to $K^{(\mathrm{MM})}_{\epsilon,2}$ from the expansion, which means calculating the limit for $r_\mathrm{t} \to \infty$. However, we can deduce the first constant

$$\Delta_{(\mathrm{MM})} = \frac{1}{7}\frac{2l^2-3}{l^2+3} \tag{109}$$

from Eq. (105). This result confirms the finding of Poniewierski and Stecki [17]. Moreover, the limit

$$\lim_{l\to\infty}\Delta_{(\mathrm{MM})} = \lim_{l\to\infty}\Delta_{[2]} = \frac{2}{7} \tag{110}$$

is the same as predicted by Priest [13].

Now we use the approximation to neglect the contribution of odd-order weight functions. The subsequent addition of higher-order terms $K^{[2n]}_{\epsilon,2}$ leaves the first constant $\Delta_{(\mathrm{MM})} \approx \tilde{\Delta}_{[2n_\mathrm{t}]} = \Delta_{[2]}$ in Eq. (108) invariant for all truncation orders $2n_\mathrm{t}$. The second constant from weight functions of even order has the form

$$\tilde{\Delta}'_{[2n_\mathrm{t}]} = \frac{3}{28}\frac{(36l^2-50)n_\mathrm{t}^2 + (162l^2-225)n_\mathrm{t} + 138l^2 - 61}{(2+n_\mathrm{t})(5+2n_\mathrm{t})(4l^2+9)} \tag{111}$$

up to at least $n_\mathrm{t} = 10$. This expression converges to the approximate

$$\Delta'_{(\mathrm{MM})} \approx \lim_{n_\mathrm{t}\to\infty}\tilde{\Delta}'_{[2n_\mathrm{t}]} = \frac{3}{28}\frac{18l^2-25}{4l^2+9}, \tag{112}$$

which shows a good numerical agreement with the result in Ref. [17], yielding the same formula for $l \to \infty$.

Note that we do not find an expansion of the form of Eq. (107) at all when using the generalized ζ correction, Eq. (52), which we discuss in Appendix B. When we include third terms, the expansion becomes ambiguous. In addition to $\bar{P}_4/\bar{P}_2$, we find a term proportional to $\bar{P}_2$, which is also of quadratic order in α.

Consider the elastic coefficients of infinitely long spherocylinders within the ζ approximation from Eq. (94). The leading terms in Eqs. (87) and (89) depend on the orientational moments I_{2n} in the same way. We easily find the ratio

$$\lim_{l\to\infty}\frac{K_1^{(\zeta)}}{K_2^{(\zeta)}} = 3 \tag{113}$$

independently of the choice for the third term. This result agrees with earlier predictions in the Onsager approximation [11–13,17,18]. To study the ratio

$$3\lim_{l\to\infty}\frac{K_3^{(\zeta)}}{K_1^{(\zeta)}} = \lim_{l\to\infty}\frac{K_3^{(\zeta)}}{K_2^{(\zeta)}} = \frac{4\left[I_4(\alpha)-I_6(\alpha)\right]}{I_2(\alpha)-2I_4(\alpha)+I_6(\alpha)}, \tag{114}$$

we consider the scaling $\alpha^2 = \alpha_1^2 l + \alpha_0^2 + \mathcal{O}(l^{-1})$ of the intrinsic order parameter α at nonzero packing fraction [51]. Expanding the moments from Eq. (68) in terms of l^{-1} yields

$$\lim_{l\to\infty}\frac{K_3^{(\zeta)}}{K_1^{(\zeta)}} = \lim_{l\to\infty}\frac{2}{3}\alpha_1^2 l = \infty. \tag{115}$$

In this case, the scaling is not compatible with the low-order elastic coefficients from Eq. (97) or Eq. (105), as the long rods are nearly perfectly aligned, i.e., $S \simeq 1$. The behavior found in Eqs. (113) and (115) appears to be universal as it does not change when adding further terms $K^{[r]}_{\epsilon,2}$. Similarly, we can show that the normalized elastic coefficients $\beta K_1 D/l$, $\beta K_2 D/l$, and $\beta K_3 D/l^2$ remain finite for $l \to \infty$. Hence, odd-order terms do not contribute in this limit.

However, the scaling in Eq. (115) contradicts the observation $K_3/K_1 = \mathcal{O}(l^2)$ made by Poniewierski [72]. We already remarked [51] that truncated FMT functionals lack a correct scaling of the orientational degrees of freedom which is remedied by the exact FMMT [59]. To check this, we examine the scaling based on the Poniewierski-Stecki equations. According to Eq. (2) the elastic coefficients only differ by a factor r_ϵ^2 in the integrand. In the limit $l \to \infty$, we only consider the terms in Eq. (76) which contain $\bar{z}$ and find $K_3/K_1 \propto r_3^2/r_1^2 = \mathcal{O}(\theta^{-2})$. Therefore, the scaling with l^1 of the ratio in Eq. (115) is a consequence of the wrong prediction $\theta = \mathcal{O}(l^{-1/2})$ using truncated functionals [51]. The full FMMT functional yields the correct $\theta = \mathcal{O}(l^{-1})$ [59,71] but does not allow the analytic study of elastic coefficients demonstrated here.

In the artificial limit of perfectly aligned bodies with $\bar{P}_{2n} \equiv 1$, the leading terms of K_1 and K_2 in the aspect ratio are identically zero for all contributions shown in Eq. (92) and Appendix B. All nonvanishing terms are of $\mathcal{O}(l^0)$. We precisely observe the opposite behavior for $K_3 = \mathcal{O}(l^2)$. Therefore, the ratio $K_3/K_1 = \mathcal{O}(l^2)$ shows the correct scaling behavior. We also see that the odd-order terms of the expansion in $K^{[r]}_{\epsilon,2}$ vanish for K_3, whereas they are of the same order of magnitude as the other contributions for splay and twist deformations. Therefore, we expect for the orientational disordered system that the even-order terms are usually sufficient to calculate K_3 with a high accuracy. As the order parameter (at given density) increases with the aspect ratio, this approximation should not

work for K_1 and K_2, except for very long rods according to the Onsager limit.

E. Numerical results

In Sec. III C, we studied analytic approximations to the Frank elastic coefficients from FMMT. Now we wish to compare these results to the full expressions $K_\epsilon^{(\mathrm{MM})}$, obtained with the numeric solution of Eq. (93). As discussed in Sec. III A regarding the equation of state, we first determine the intrinsic order parameter α from Eq. (71) using the generalized ζ correction, Eq. (52), truncated at $n_\mathrm{t} = 50$. Then we evaluate Eq. (86) numerically and add the analytic result from Eq. (89) accounting for the third term. To do so, we use Monte Carlo integration as for the nematic bulk phase. Due to the more general integrand in Eq. (78), we need to include the integrals over the orientational angles ϕ_1 and ϕ_2 to our numerical procedure. We calculate this eight-dimensional integral, such that the numerical error is smaller than the linewidth in our figures and the uncertainty of shown numbers is at least 1 in the last digit.

In Fig. 3, we study the convergence of the expansion from Eq. (95). We first only consider the even-order terms by temporarily setting $m_\mathrm{t} = 0$. We see that the expansion converges as rapidly as for the nematic equation of state in Fig. 2, such that truncation after $n_\mathrm{t} = 7$ is sufficient. Following the discussion in Sec. III C, the limit $n_\mathrm{t} \to \infty$ corresponds to an approximation for $K_\epsilon^{(\mathrm{MM})}$, where the contribution of $-2r_\epsilon r'_\epsilon$ in Eq. (79) is neglected, as we ignore all odd $K_{\epsilon,2}^{[2n+1]}$. Surprisingly, the deviation from the correct mixed measure result is nearly negligible for K_3, as shown in Fig. 3(b). This result is only easily explained for long rods, as in the previous section. However, we find the significant error of 26% for K_1 and 19% for K_2 (not shown) at $l = 5$ and $\eta = 0.5$. In general, this deviation becomes smaller when we increase the aspect ratio and decrease the nematic order parameter, in accordance with our analytic predictions from Sec. III C.

To approach the exact result for any deformation and aspect ratio, we need to include the odd-order terms to the expansion in Eq. (95). While we may keep the generalized ζ correction for the even-order terms, we have no such correction [51] for the odd orders. Consequently, this sum converges slowly and we require $m_\mathrm{t} = 12$ in addition to the sufficiently large $n_\mathrm{t} = 7$ to obtain a good agreement with the full numeric result for K_1 in Fig. 3(a). Within the stability range of the nematic phase [59], Fig. 3 reveals that we can truncate this expansion in a reasonably good approximation at $n_\mathrm{t} = m_\mathrm{t} = 3$. In this case, we only need the explicit formulas shown in Appendix B. Therefore, we possess a useful analytic approximation for the Frank elastic coefficients, given by Eq. (95).

In Table II, we compare our results for the elastic coefficients obtained with different variants of FMMT to computer simulations [33,34] and DFT results [22,24] for hard spherocylinders with an aspect ratio of $l = 5$. The nematic order parameter $S \approx 0.73$ is found in simulations after equilibration of a system with initial packing fraction $\eta = 0.4418$ [33,34]. Using both values as an input for our calculations violates the equilibrium condition from Eq. (71). However, this strategy, providing the possibility to cross-check future results with our analytic expansion, is worth being

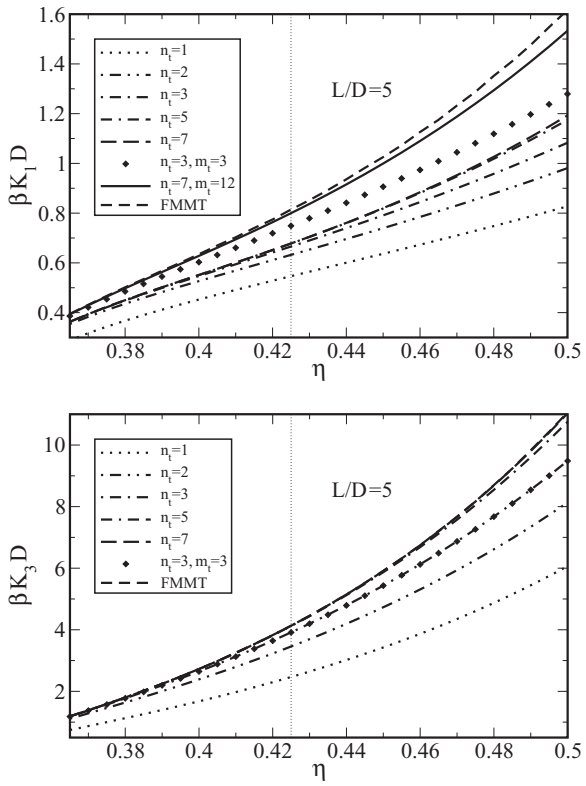

FIG. 3. (a) Splay elastic constant K_1 and (b) bend elastic constant K_3 as a function of the packing fraction η. We compare the analytic formulas from the expansion in Eq. (95) at different truncation orders n_t and m_t to the numeric FMMT values according to Eq. (93), which involves the full mixed weight function. Unless mentioned otherwise, $m_\mathrm{t} = 0$. As in Fig. 2, we use $\phi_3^{(\mathrm{TR})}$ and verify a quick convergence of the even-order terms in Eq. (95), setting $m_\mathrm{t} = 0$. As our best analytic approximation for K_1, we add odd-order terms up to $m_\mathrm{t} = 12$ to the result for $n_\mathrm{t} = 7$. The result for K_3 for $m_\mathrm{t} = 0$ and $n_\mathrm{t} = 7$ is indistinguishable from the full FMMT result. The diamonds denote the result, which we obtain using only the formulas we provide in Appendix B. The nematic phase is stable to the left of the vertical dashed line.

compared to the simulations. The third term $\phi_3^{(\mathrm{TR})}$ from Eq. (55) yields a good agreement for K_1 and K_2, whereas K_3 is overestimated. For $\phi_3^{(\mathrm{T})}$ from Eq. (56), the values are significantly smaller and only the result for K_3 appears reasonable. It is difficult to draw further conclusions from this single available data point.

As we already see from the DFT results of Somoza and Tarazona [22] and Poniewierski and Hołyst [24], the equilibrium nematic order parameter S of different approaches may differ noticeably. In our calculation using $\phi_3^{(\mathrm{TR})}$ or $\phi_3^{(\mathrm{T})}$, its value corresponding to $\eta = 0.4418$ is respectively larger or smaller than in all considered references. Therefore, a comparison becomes difficult. We also fix the order parameter and calculate the corresponding equilibrium density according to Eq. (71). This strategy provides the best basis for a comparison. The elastic coefficients are much more sensitive to changes in the nematic order parameter than in the density, which we notice from the different results in Table II. Quantitatively, our results seem to be closer to the simulations at the same value of S when

TABLE II. Elastic coefficients of hard spherocylinders with aspect ratio $l = 5$. We compare FMT to different references using the ζ approximation in Eq. (94) and the exact expression for the second term in Eq. (93) together with both third terms $\phi_3^{(\mathrm{TR})}$ and $\phi_3^{(\mathrm{T})}$ from Eqs. (55) and (56). Our input parameters are constrained by the equilibrium condition, Eq. (71). The first row of our results for each functional is at fixed packing fraction $\eta = 0.4418$. The dashes in the seventh and tenth row indicate that the nematic phase is unstable in this case. We show further results corresponding to the fixed nematic order parameters $S = 0.727$ and $S = 0.791$, obtained in other references for $\eta = 0.4418$. The simulation data are from the works of Allen and Frenkel (multiplied by 9/4) [33] and more recently Fischermeier *et al.* (using two different fit methods) [34], where the number in brackets denotes the error in the last digit. The DFT results are by Poniewierski and Hołyst [24] and Somoza and Tarazona [22]. In the last two rows, we show our (nonequilibrium) FMT results imposing both the packing fraction and the nematic order parameter.

K_ϵ	η	S	$\beta K_1 D$	$\beta K_2 D$	$\beta K_3 D$
	0.4418	0.901	0.951	0.457	5.276
FMMT, TR	0.3658	0.727	0.401	0.181	1.222
	0.3809	0.791	0.507	0.233	1.836
	0.4418	0.849	0.607	0.309	3.089
$\zeta = 5/4$, TR	0.3831	0.727	0.382	0.176	1.211
	0.4063	0.791	0.477	0.229	1.863
	0.4418	0			
FMMT, T	0.4992	0.727	0.590	0.277	1.735
	0.5181	0.791	0.761	0.360	2.593
	0.4418	0			
$\zeta = 5/4$, T	0.5547	0.727	1.553	0.699	4.952
	0.6071	0.791	2.470	1.148	9.721
	0.4418	0.652	0.366	0.174	0.955
$\zeta = 1.6$, T	0.4733	0.727	0.480	0.238	1.499
	0.5174	0.791	0.622	0.325	2.377
AF [33]	0.4418	0.73	0.83(25)	0.59(7)	1.10(11)
Fi [34]	0.4418	0.727	0.763(45)	0.348(24)	1.226(45)
Fi [34]	0.4418	0.727	0.812(19)	0.352(16)	1.583(27)
PH [24]	0.4418	0.728	0.513	0.239	1.526
ST[22]	0.4418	0.791	0.630	0.297	2.403
FMMT, TR	0.4418	0.727	0.741	0.332	2.274
FMMT, T	0.4418	0.727	0.423	0.198	1.247

we use Tarazona's expression $\phi_3^{(\mathrm{T})}$ in the third term. However, this version of the functional yields a diverging free energy per particle for infinitely long rods at finite packing fraction [51] and therefore needs to be queried. In particular, the poor description of the equation of state results in an unstable nematic phase at the packing fraction $\eta = 0.4418$. We also consider the ζ correction, Eq. (94), for the truncated expansion in Table II. The semiempirical choice $\zeta = 5/4$ [46,51], which is convenient to describe the isotropic-nematic transition with $\phi_3^{(\mathrm{TR})}$, does not provide a sufficiently good approximation for FMMT (see also the results for $n_t = 1$ in Fig. 3), and neither does the fit value $\zeta = 1.6$ [46] with $\phi_3^{(\mathrm{T})}$.

Figure 4 shows the results for $K_\epsilon^{(\mathrm{MM})}(\eta)$ and $K_\epsilon^{(\mathrm{MM})}(S)$ at $l = 5$ using the full FMMT functional with the third term by Tarazona and Rosenfeld, as considered in Ref. [59]. Indeed,

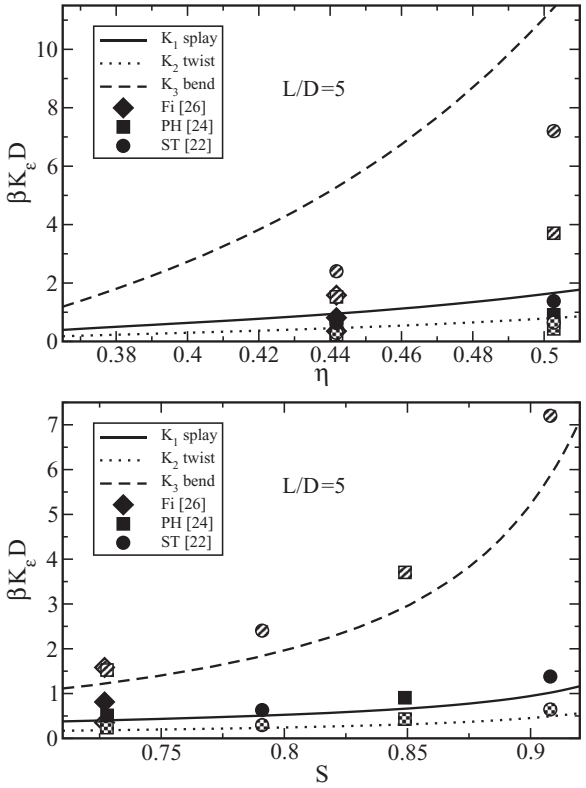

FIG. 4. Elastic coefficients $K_\epsilon^{(\mathrm{MM})}$ of hard spherocylinders using $\phi_3^{(\mathrm{TR})}$ with an aspect ratio of $l = 5$. The solid, dotted, and dashed lines or symbols correspond to splay, twist, and bend, respectively. As a function of (a) the packing fraction η and (b) the nematic order parameter S, we compare our FMMT results to computer simulations for $\eta = 0.4418$ [34] and other DFT values [22,24] corresponding to $\eta = 0.4418$ and $\eta = 0.5181$. Note that these functionals, as well as FMMT, predict different equilibrium order parameters.

we see that the nematic order parameter S is more suitable for this plot, as the two different DFT results [22,24] fit together in a better way and confirm the qualitative behavior of our predictions. We also see that the bend constant K_3 increases more rapidly with S than K_1 and K_2, which we expect from the discussion of the limit $S \to 1$ in Sec. III D. In Fig. 5, we compare the behavior of the elastic coefficients for different aspect ratios l. We always observe the relation $K_3 > K_1 > K_2$ [15]. The twist constant K_2 exhibits a similar behavior as K_1 for splay, whereas the bend constant K_3 increases more rapidly with larger l. Hence, the ratios K_3/K_1 and K_3/K_2 appear to diverge for $l \to \infty$, whereas K_1/K_2 remains finite, as we predicted analytically by Eqs. (115) and (113).

IV. SUMMARY

In this work, we explored the foundation of FMT, providing some mathematical essentials from integral geometry. We defined the geometric weight functions in a mathematically convenient way through curvature measures and introduced the notion of mixed measures as a new type of building block. Within this family of density functionals, we found a general approach to calculate the Frank elastic coefficients in the nematic phase of arbitrarily shaped hard bodies.

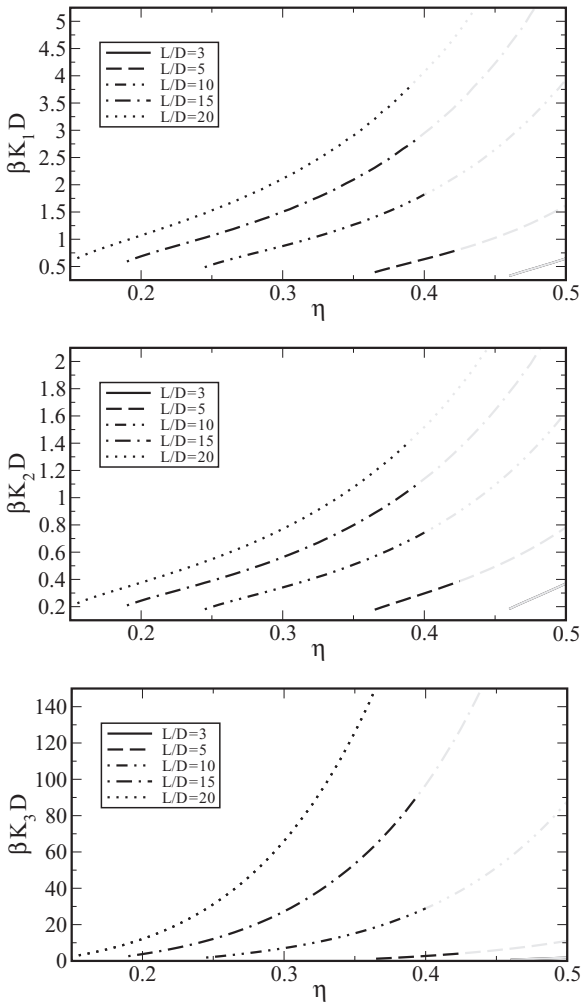

FIG. 5. (a) Splay, (b) twist, and (c) bend elastic coefficients of hard spherocylinders as a function of the packing fraction η. We show the FMMT results $K_\epsilon^{(\mathrm{MM})}$ using $\phi_3^{(\mathrm{TR})}$ for different aspect ratios $l = L/D$. The gray extension is beyond the stability limit of the nematic phase [59].

This application demonstrates the two main purposes of our new FMMT. The first one is to verify the convergence of expansions, which are easier to implement. For the present problem, we provide an analytic series representation. However, we should consider a systematic expansion including odd-order terms [65] to improve the convergence for short rods. The shortcomings of the ζ correction for inhomogeneous systems [51,59] also show up in this work. Second, this work constitutes an example where the factorization of a two-body measure into quantities of one body [46,47], which is desirable regarding the numerical implementation, actually complicates the calculation. When expanding the functional, the analytic evaluation of higher-order contributions is considerably easier with one eight-dimensional integral involving a mixed weight function than several individual four-dimensional integrals for each component of a rank-r tensor.

For the first time, we present a closed analytical solution of the Poniewierski-Stecki equations beyond the Onsager approximation. These expressions still depend implicitly on the nematic order parameter $S(\alpha)$, which is found numerically by minimizing the free energy at given density with respect to α. An interesting application of our formulas is to input both the packing fraction and the nematic order parameter from simulations or experiments as an alternative to the (highly involved) direct measurement of the elastic constants. However, there are not enough simulation data available to make a statement about the accuracy of such an approach.

Regarding the density functional, we can think of some possible improvement in future work. Its third term has a remarkable influence on the values of the elastic coefficients as it does for the equation of state [51]. The current expression by Tarazona and Rosenfeld [57] is the only one including at most rank-2 tensors to account for extremely confined systems and the phase diagram of very long rods, while predicting the same equation of state as FMT in the hard-sphere limit [51]. For a quantitative improvement of our results, the third term needs to be revisited, which appears to be a very elaborate task. A better approximation could involve a parameter to fix the third virial coefficient of the monodisperse system [51,73] or, more desirably, an additional mixed weighted density or tensors of higher rank. In any case, the expression for the elastic coefficients from Eq. (3) is universal and can be used for any FMT-like functional. Moreover, we expect that Eq. (95) can be used to calculate analytic elastic coefficients for other systems than a fluid of hard spherocylinders.

ACKNOWLEDGMENTS

The authors would like to thank Daniel Hug for introducing us to mixed measures and communicating his results for the representations in two and three dimensions. Financial support by the DFG under Grant No. Me1361/12 as part of the Research Unit "Geometry and Physics of Spatial Random Systems" is gratefully acknowledged.

APPENDIX A: INVERSION FORMULA

In this section, we derive Eq. (33). We start by integrating both sides of Eq. (14) over all translations $\mathbf{x}$ of the body K in a Borel set $B \subset \mathbb{R}^d$, obtaining

$$\int_B d\mathbf{x} \sum_{\nu=0}^{d} \kappa_{d-\nu} \varrho^{d-\nu} \Phi_\nu(K+\mathbf{x}, A) \tag{A1}$$

$$= \int_B d\mathbf{x} \lambda(\mathbf{q} \in K_\varrho : \mathbf{p}(K+\mathbf{x}, \mathbf{q}) \in A). \tag{A2}$$

Subsequently, we write the d-dimensional volume as an integral over q to obtain

$$\iint_{\mathbb{R}^d \times \mathbb{R}^d} d\mathbf{x} d\mathbf{q} \mathbb{I}_B(\mathbf{x}) \mathbb{I}_{K_\varrho}(\mathbf{q}-\mathbf{x}) \mathbb{I}_A[\mathbf{p}(K+\mathbf{x}, \mathbf{q})], \tag{A3}$$

where we used the indicator function $\mathbb{I}_A(\mathbf{x})$ which is 1 if $\mathbf{x} \in A$ and 0 otherwise. Now we perform a point reflection of the body, as depicted in Fig. 6, and a variable substitution, $(\mathbf{x}, \mathbf{q}) \to (\mathbf{r}, \mathbf{z}) = [\mathbf{p}(K+\mathbf{x}, \mathbf{q}), \mathbf{x}+\mathbf{r}-\mathbf{q}]$, to write Eq. (A3) as

$$\iint_{\mathbb{R}^d \times \mathbb{R}^d} d\mathbf{r} d\mathbf{z} \mathbb{I}_B[\mathbf{p}(\mathbf{r}-K, \mathbf{z})] \mathbb{I}_{-K_\varrho}(\mathbf{z}-\mathbf{r}) \mathbb{I}_A(\mathbf{r}), \tag{A4}$$

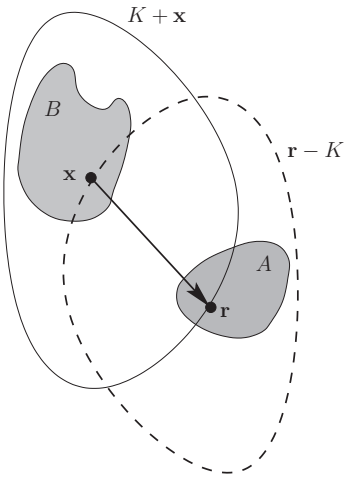

FIG. 6. Illustration of the original body $K+\mathbf{x}$ (solid loop), its point inversion $\mathbf{r}-K$ (dashed loop), and the two Borel sets A and B (shaded regions). The arrow denotes $\mathbf{r}-\mathbf{x}=\mathbf{p}(K+\mathbf{x},\mathbf{y})-\mathbf{x}=\mathbf{r}-\mathbf{p}(\mathbf{r}-K,\mathbf{z})$.

where we used $-\mathbf{p}(K,\mathbf{x}')=\mathbf{p}(-K,-\mathbf{x}')$ for any point $\mathbf{x}'$, which implies $\mathbf{x}=\mathbf{z}+\mathbf{q}-\mathbf{r}=\mathbf{p}(\mathbf{r}-K,\mathbf{z})$.

Reversing the steps leading to Eqs. (A4) and (A3), we obtain the identity

$$\int_A d\mathbf{r}\sum_{\nu=0}^{d}\kappa_{d-\nu}\varrho^{d-\nu}\Phi_\nu(\mathbf{r}-K,B), \tag{A5}$$

which has to be equal to Eq. (A1) for all ϱ, such that the identity must also hold for all terms individually:

$$\int_B d\mathbf{x}\Phi_\nu(K+\mathbf{x},A)=\int_A d\mathbf{r}\Phi_\nu(\mathbf{r}-K,B). \tag{A6}$$

This can be written as Eq. (33) by setting $A=d\mathbf{r}$, $B=d\mathbf{r}_1$ and $K=\mathcal{I}(\mathbf{0},-\mathbf{y})=\mathcal{I}(\mathbf{x},\mathbf{x}-\mathbf{y})-\mathbf{x}$ and using

$$\begin{aligned}\mathbf{r}-\mathcal{I}(\mathbf{0},-\mathbf{y})&=\mathbf{r}-[\mathcal{B}_i(\mathbf{0})\cap(\mathcal{B}_i(\mathbf{0})-\mathbf{y})]\\&=[\mathbf{r}-\mathcal{B}_i(\mathbf{0})]\cap[\mathbf{r}-\mathcal{B}_i(\mathbf{0})+\mathbf{y}]=\bar{\mathcal{I}}(\mathbf{r},\mathbf{r}+\mathbf{y}).\end{aligned} \tag{A7}$$

APPENDIX B: HIGHER-ORDER TERMS OF THE ELASTIC COEFFICIENTS

In this Appendix, we list additional contributions to the Frank elastic coefficients in terms of nematic order parameters $\bar{P}_{2n}$ from Eq. (70). So far, we only wrote the formula for the leading term $K^{[2]}_{\epsilon,2}$ in Eq. (92) to make Sec. III C more compact. In this alternative representation, the formulas in Eq. (89) read

$$\begin{aligned}\beta K^{(\mathrm{TR})}_{1,3}D&=\frac{81\eta^3l^2S(4S+3\bar{P}_4)}{28\pi(3l+2)^3(1-\eta)^2}+\frac{81\eta^3l^3S\left(320S+9\bar{P}_4+325S^2+396\bar{P}_4^2-210S\bar{P}_6\right)}{2240\pi(3l+2)^3(1-\eta)^2}\\&\quad+\frac{81\eta^3l^4S(S-\bar{P}_4)}{7\pi(3l+2)^3(1-\eta)^2}+\frac{81\eta^3l^5S\left(80S-3\bar{P}_4-15S^2-132\bar{P}_4^2+70S\bar{P}_6\right)}{560\pi(3l+2)^3(1-\eta)^2},\\\beta K^{(\mathrm{TR})}_{2,3}D&=\frac{81\eta^3l^2S(6S+\bar{P}_4)}{28\pi(3l+2)^3(1-\eta)^2}+\frac{81\eta^3l^3S\left(480S+3\bar{P}_4+295S^2+132\bar{P}_4^2-70S\bar{P}_6\right)}{2240\pi(3l+2)^3(1-\eta)^2}\\&\quad+\frac{27\eta^3l^4S(S-\bar{P}_4)}{7\pi(3l+2)^3(1-\eta)^2}+\frac{27\eta^3l^5S\left(80S-3\bar{P}_4-15S^2-132\bar{P}_4^2+70S\bar{P}_6\right)}{560\pi(3l+2)^3(1-\eta)^2},\\\beta K^{(\mathrm{TR})}_{3,3}D&=\frac{81\eta^3l^2S(S-\bar{P}_4)}{7\pi(3l+2)^3(1-\eta)^2}+\frac{81\eta^3l^3S\left(80S-3\bar{P}_4-15S^2-132\bar{P}_4^2+70S\bar{P}_6\right)}{560\pi(3l+2)^3(1-\eta)^2}\\&\quad+\frac{27\eta^3l^4S(3S+4\bar{P}_4)}{7\pi(3l+2)^3(1-\eta)^2}+\frac{27\eta^3l^5S\left(60S+3\bar{P}_4+85S^2-132\bar{P}_4^2+70S\bar{P}_6\right)}{140\pi(3l+2)^3(1-\eta)^2},\end{aligned} \tag{B1}$$

or

$$\begin{aligned}\beta K^{(\mathrm{T})}_{1,3}D&=-\frac{81\eta^3l^3S^2[(4S+3\bar{P}_4)+4l^2(S-\bar{P}_4)]}{112\pi(3l+2)^3(1-\eta)^2},\\\beta K^{(\mathrm{T})}_{2,3}D&=-\frac{27\eta^3l^3S^2[(18S+3\bar{P}_4)+4l^2(S-\bar{P}_4)]}{112\pi(3l+2)^3(1-\eta)^2},\\\beta K^{(\mathrm{T})}_{3,3}D&=-\frac{27\eta^3l^3S^2[3(S-\bar{P}_4)+l^2(3S+4\bar{P}_4)]}{28\pi(3l+2)^3(1-\eta)^2},\end{aligned} \tag{B2}$$

when we use the respective factor from Eq. (90) or Eq. (91). We also find analytic formulas for the contributions $K^{[r]}_{\epsilon,2}$ from Eq. (85), corresponding to the expansion of the mixed weight function from Eq. (44).

The first two even next-to-leading terms after Eq. (92) read

$$\begin{aligned}
\beta K^{[4]}_{1,2} D &= \frac{3\eta^2 l^2\left(1056S^2 + 2277S\bar{P}_4 + 4801\bar{P}_4^2 + 2646\bar{P}_4\bar{P}_6\right)}{4312\pi(1-\eta)(3l+2)^2} + \frac{9\eta^2 l^4\left(132S^2 - 187S\bar{P}_4 + 300\bar{P}_4^2 - 245\bar{P}_4\bar{P}_6\right)}{2156\pi(1-\eta)(3l+2)^2},\\
\beta K^{[4]}_{2,2} D &= \frac{9\eta^2 l^2\left(682S^2 + 253S\bar{P}_4 + 927\bar{P}_4^2 + 294\bar{P}_4\bar{P}_6\right)}{4312\pi(1-\eta)(3l+2)^2} + \frac{3\eta^2 l^4\left(132S^2 - 187S\bar{P}_4 + 300\bar{P}_4^2 - 245\bar{P}_4\bar{P}_6\right)}{2156\pi(1-\eta)(3l+2)^2},\\
\beta K^{[4]}_{3,2} D &= \frac{3\eta^2 l^2\left(264S^2 - 759S\bar{P}_4 + 1377\bar{P}_4^2 - 882\bar{P}_4\bar{P}_6\right)}{1078\pi(1-\eta)(3l+2)^2} + \frac{3\eta^2 l^4\left(198S^2 + 374S\bar{P}_4 + 555\bar{P}_4^2 + 490\bar{P}_4\bar{P}_6\right)}{1078\pi(1-\eta)(3l+2)^2}
\end{aligned} \tag{B3}$$

and

$$\begin{aligned}
\beta K^{[6]}_{1,2} D &= \frac{3\eta^2 l^2\left(402\,688S^2 + 1\,228\,656S\bar{P}_4 + 2\,995\,824\bar{P}_4^2 + 2\,474\,304\bar{P}_4\bar{P}_6 + 2\,139\,683\bar{P}_6^2 + 1\,164\,240\bar{P}_6\bar{P}_8\right)}{4\,932\,928\pi(1-\eta)(3l+2)^2}\\
&\quad + \frac{9\eta^2 l^4\left(12\,584S^2 - 21\,164S\bar{P}_4 + 46\,800\bar{P}_4^2 - 46\,795\bar{P}_4\bar{P}_6 + 31\,213\bar{P}_6^2 - 22\,638\bar{P}_6\bar{P}_8\right)}{616\,616\pi(1-\eta)(3l+2)^2},\\
\beta K^{[6]}_{2,2} D &= \frac{3\eta^2 l^2\left(390\,104S^2 + 204\,776S\bar{P}_4 + 867\,672\bar{P}_4^2 + 412\,384\bar{P}_4\bar{P}_6 + 474\,565\bar{P}_6^2 + 194\,040\bar{P}_6\bar{P}_8\right)}{2\,466\,464\pi(1-\eta)(3l+2)^2}\\
&\quad + \frac{3\eta^2 l^4\left(12\,584S^2 - 21\,164S\bar{P}_4 + 46\,800\bar{P}_4^2 - 46\,795\bar{P}_4\bar{P}_6 + 31\,213\bar{P}_6^2 - 22\,638\bar{P}_6\bar{P}_8\right)}{616\,616\pi(1-\eta)(3l+2)^2},\\
\beta K^{[6]}_{3,2} D &= \frac{3\eta^2 l^2\left(6292S^2 - 25\,597S\bar{P}_4 + 53\,703\bar{P}_4^2 - 51\,548\bar{P}_4\bar{P}_6 + 41\,405\bar{P}_6^2 - 24\,255\bar{P}_6\bar{P}_8\right)}{616\,616\pi(1-\eta)(3l+2)^2}\\
&\quad + \frac{3\eta^2 l^4\left(37\,752S^2 + 84\,656S\bar{P}_4 + 173\,160\bar{P}_4^2 + 187\,180\bar{P}_4\bar{P}_6 + 120\,393\bar{P}_6^2 + 90\,552\bar{P}_6\bar{P}_8\right)}{4\,932\,928\pi(1-\eta)(3l+2)^2}.
\end{aligned} \tag{B4}$$

Compared to Eq. (92), we find the additional order parameters $\bar{P}_6$ and $\bar{P}_8$. Note that these expressions for are not unique, as we find relations like

$$715S\bar{P}_6 - 525\bar{P}_4^2 + 104\bar{P}_4\bar{P}_6 - 910\bar{P}_6^2 + 616\bar{P}_4\bar{P}_8 = 0, \tag{B5}$$

using our representations from Eq. (68) with Eq. (70) in terms of α. We choose the formulas with the least number of terms including the highest order parameter $\bar{P}_{r+2}$. The odd-order elastic coefficients [note the minus sign in Eq. (45) for odd values of r]

$$\begin{aligned}
\beta K^{[3]}_{1,2} D &= \frac{45\eta^2 l^2\left(32S^2 + 69S\bar{P}_4 + 46\bar{P}_4^2\right)}{784\pi(3l+2)^2(1-\eta)},\\
\beta K^{[3]}_{2,2} D &= \frac{45\eta^2 l^2\left(20S^2 + 23S\bar{P}_4 + 6\bar{P}_4^2\right)}{784\pi(3l+2)^2(1-\eta)},\\
\beta K^{[3]}_{3,2} D &= \frac{45\eta^2 l^2\left(8S^2 - 23S\bar{P}_4 + 15\bar{P}_4^2\right)}{196\pi(3l+2)^2(1-\eta)},
\end{aligned} \tag{B6}$$

$$\begin{aligned}
\beta K^{[5]}_{1,2} D &= \frac{3\eta^2 l^2\left(19\,360S^2 + 41\,745S\bar{P}_4 + 55\,956\bar{P}_4^2 + 60\,711\bar{P}_4\bar{P}_6 + 35\,672\bar{P}_6^2\right)}{94864\pi(1-\eta)(3l+2)^2},\\
\beta K^{[5]}_{2,2} D &= \frac{3\eta^2 l^2\left(12\,100S^2 + 13\,915S\bar{P}_4 + 18\,036\bar{P}_4^2 + 20\,237\bar{P}_4\bar{P}_6 + 6860\bar{P}_6^2\right)}{94864\pi(1-\eta)(3l+2)^2},\\
\beta K^{[5]}_{3,2} D &= \frac{3\eta^2 l^2\left(4840S^2 - 13\,915S\bar{P}_4 + 17\,307\bar{P}_4^2 - 20\,237\bar{P}_4\bar{P}_6 + 12\,005\bar{P}_6^2\right)}{23\,716\pi(1-\eta)(3l+2)^2},
\end{aligned} \tag{B7}$$

and

$$\beta K_{1,2}^{[7]} D = \frac{3\eta^2 l^2 \left(1\,830\,400 S^2 + 3\,946\,800 S \bar{P}_4 + 7\,131\,360 \bar{P}_4^2 + 9\,713\,760 \bar{P}_4 \bar{P}_6 + 7\,977\,788 \bar{P}_6^2 + 4\,846\,149 \bar{P}_6 \bar{P}_8 + 2\,706\,858 \bar{P}_8^2\right)}{19\,731\,712\pi(1-\eta)(3l+2)^2},$$

$$\beta K_{2,2}^{[7]} D = \frac{3\eta^2 l^2 \left(1\,144\,000 S^2 + 1\,315\,600 S \bar{P}_4 + 2\,648\,160 \bar{P}_4^2 + 3\,237\,920 \bar{P}_4 \bar{P}_6 + 2\,145\,416 \bar{P}_6^2 + 1\,615\,383 \bar{P}_6 \bar{P}_8 + 611\,226 \bar{P}_8^2\right)}{19\,731\,712\pi(1-\eta)(3l+2)^2},$$

$$\beta K_{3,2}^{[7]} D = \frac{3\eta^2 l^2 \left(457\,600 S^2 - 1\,315\,600 S \bar{P}_4 + 2\,175\,120 \bar{P}_4^2 - 3\,237\,920 \bar{P}_4 \bar{P}_6 + 2\,619\,344 \bar{P}_6^2 - 1\,615\,383 \bar{P}_6 \bar{P}_8 + 916\,839 \bar{P}_8^2\right)}{4\,932\,928\pi(1-\eta)(3l+2)^2}, \tag{B8}$$

include order parameters up to $\bar{P}_{r+1}$. We also determined higher-order terms, but the formulas are too long to be included here.

Ignoring the odd-order contributions $K_{\epsilon,2}^{[2n+1]}$ completely, it appears convenient to add up the even-order terms according to the generalized ζ correction from Eq. (52). Interestingly, we find that then the leading order, which is proportional to $\bar{P}_{2(n_t-1)} \bar{P}_{2n_t}$, cancels when calculating the average constant $\bar{K}_\epsilon$, which is then proportional to $\bar{P}_{2n_t}^2$. Hence, the ratios diverge in the limit $\alpha \to 0$ and this approach fails to predict the expansion defined in Eq. (107).

[1] P. G. de Gennes and J. Prost, *The Physics of Liquid Crystals* (Clarendon Press, Oxford, 1993).
[2] J. P. F. Lagerwall and G. Scalia, Curr. Appl. Phys. **12**, 1387 (2012).
[3] H. Kawamoto, Proc. IEEE **90**, 460 (2002).
[4] F. C. Frank, Discuss. Faraday Soc. **25**, 19 (1958).
[5] R. B. Meyer, F. Lonberg, V. Taratuta, S. Fraden, S.-D. Lee, and A. J. Hurd, Faraday Discuss. Chem. Soc. **79**, 125 (1985).
[6] A. J. Hurd, S. Fraden, F. Lonberg, and R. B. Meyer, J. Phys. (Paris) **46**, 905 (1985).
[7] D. van der Beek, P. Davidson, H. H. Wensink, G. J. Vroege, and H. N. W. Lekkerkerker, Phys. Rev. E **77**, 031708 (2008).
[8] A. A. Verhoeff, R. H. J. Otten, P. van der Schoot, and H. N. W. Lekkerkerker, J. Phys. Chem. B **113**, 3704 (2009).
[9] L. Onsager, Ann. NY Acad. Sci. **51**, 627 (1949).
[10] L. Mederos, E. Velasco, and Y. Martínez-Ratón, J. Phys.: Condens. Matter **26**, 463101 (2014).
[11] J. P. Straley, Phys. Rev. A **8**, 2181 (1973).
[12] S.-D. Lee and R. B. Meyer, J. Chem. Phys. **84**, 3443 (1986).
[13] R. G. Priest, Phys. Rev. A **7**, 720 (1973).
[14] P. G. de Gennes, Mol. Cryst. Liq. Cryst. (1969-1991) **12**, 193 (1971).
[15] M. Kröger and P. Ilg, J. Chem. Phys. **127**, 034903 (2007).
[16] R. Evans, Adv. Phys. **28**, 143 (1979).
[17] A. Poniewierski and J. Stecki, Mol. Phys. **38**, 1931 (1979).
[18] J. Stecki and A. Poniewierski, Mol. Phys. **41**, 1451 (1980).
[19] J. D. Parsons, Phys. Rev. A **19**, 1225 (1979).
[20] N. F. Carnahan and K. E. Starling, J. Chem. Phys. **51**, 635 (1969).
[21] S.-D. Lee, Phys. Rev. A **39**, 3631 (1989).
[22] A. M. Somoza and P. Tarazona, Phys. Rev. A **40**, 6069 (1989).
[23] A. M. Somoza and P. Tarazona, Mol. Phys. **72**, 911 (1991).
[24] A. Poniewierski and R. Hołyst, Phys. Rev. A **41**, 6871 (1990).
[25] A. Avazpour and M. Moradi, Physica B **392**, 242 (2007).
[26] R. Pynn, J. Chem. Phys. **60**, 4579 (1974).
[27] M. Baus, J.-L. Colot, X.-G. Wu, and H. Xu, Phys. Rev. Lett. **59**, 2184 (1987).
[28] J. F. Marko, Phys. Rev. A **39**, 2050 (1989).
[29] A. Avazpour, V. Mahdavi, and L. Avazpour, Phys. Rev. E **82**, 041701 (2010).
[30] Y. Singh and K. Singh, Phys. Rev. A **33**, 3481 (1986).
[31] Y. Singh, S. Singh, and K. Rajesh, Phys. Rev. A **45**, 974 (1992).
[32] A. Srivastava and S. Singh, J. Phys.: Condens. Matter **16**, 7169 (2004).
[33] M. P. Allen and D. Frenkel, Phys. Rev. A **37**, 1813 (1988); **42**, 3641(E) (1990).
[34] E. Fischermeier, D. Bartuschat, T. Preclik, M. Marechal, and K. Mecke, Comput. Phys. Commun. **185**, 3156 (2014).
[35] B. Tjipto-Margo, G. T. Evans, M. P. Allen, and D. Frenkel, J. Phys. Chem. **96**, 3942 (1992).
[36] N. H. Phuong, G. Germano, and F. Schmid, J. Chem. Phys. **115**, 7227 (2001).
[37] P. A. O'Brien, M. P. Allen, D. L. Cheung, M. Dennison, and A. Masters, Phys. Rev. E **78**, 051705 (2008).
[38] N. H. Phuong, G. Germano, and F. Schmid, Comput. Phys. Commun. **147**, 350 (2002).
[39] Y. Rosenfeld, Phys. Rev. Lett. **63**, 980 (1989).
[40] J. K. Percus and G. J. Yevick, Phys. Rev. **110**, 1 (1958).
[41] J. L. Lebowitz, Phys. Rev. **133**, A895 (1964).
[42] R. Roth, R. Evans, A. Lang, and G. Kahl, J. Phys.: Condens. Matter **14**, 12063 (2002).
[43] H. Hansen-Goos and R. Roth, J. Phys.: Condens. Matter **18**, 8413 (2006).
[44] Y. Rosenfeld, Phys. Rev. E **50**, R3318 (1994).
[45] Y. Rosenfeld, Mol. Phys. **86**, 637 (1995).
[46] H. Hansen-Goos and K. Mecke, Phys. Rev. Lett. **102**, 018302 (2009).
[47] H. Hansen-Goos and K. Mecke, J. Phys.: Condens. Matter **22**, 364107 (2010).
[48] M. Marechal, H. H. Goetzke, A. Härtel, and H. Löwen, J. Chem. Phys. **135**, 234510 (2011).
[49] R. Wittmann and K. Mecke, J. Chem. Phys. **140**, 104703 (2014).
[50] M. Marechal and H. Löwen, Phys. Rev. Lett. **110**, 137801 (2013).
[51] R. Wittmann, M. Marechal, and K. Mecke, J. Chem. Phys. **141**, 064103 (2014).
[52] A. Esztermann, H. Reich, and M. Schmidt, Phys. Rev. E **73**, 011409 (2006).
[53] Y. Martínez-Ratón, J. A. Capitán, and J. A. Cuesta, Phys. Rev. E **77**, 051205 (2008).
[54] J. A. Capitán, Y. Martínez-Ratón, and J. A. Cuesta, J. Chem. Phys. **128**, 194901 (2008).

[55] Y. Rosenfeld, M. Schmidt, H. Löwen, and P. Tarazona, J. Phys.: Condens. Matter **8**, L577 (1996).
[56] Y. Rosenfeld, M. Schmidt, H. Löwen, and P. Tarazona, Phys. Rev. E **55**, 4245 (1997).
[57] P. Tarazona and Y. Rosenfeld, Phys. Rev. E **55**, R4873 (1997).
[58] P. Tarazona, Phys. Rev. Lett. **84**, 694 (2000).
[59] R. Wittmann, M. Marechal, and K. Mecke, Europhys. Lett. **109**, 26003 (2015).
[60] R. Schneider and W. Weil, *Stochastic and integral geometry* (Springer, Berlin, 2008).
[61] K. R. Mecke, Lect. Notes Phys. **554**, 111 (2000).
[62] H. Hadwiger, *Vorlesungen über Inhalt, Oberfläche und Isoperimetrie* (Springer, Heidelberg, 1957).
[63] R. M. Gibbons, Mol. Phys. **17**, 81 (1969).
[64] D. Hug (private communication).
[65] M. S. Wertheim, Mol. Phys. **83**, 519 (1994).
[66] G. E. Schröder-Turk, W. Mickel, S. C. Kapfer, F. M. Schaller, B. Breidenbach, D. Hug, and K. Mecke, New J. Phys. **15**, 083028 (2013).
[67] H. Reiss, H. L. Frisch, E. Helfand, and J. L. Lebowitz, J. Chem. Phys. **32**, 119 (1960).
[68] S. Korden, Phys. Rev. E **85**, 041150 (2012).
[69] M. Marechal, S. Korden, and K. Mecke, Phys. Rev. E **90**, 042131 (2014).
[70] S. C. McGrother, D. C. Williamson, and G. Jackson, J. Chem. Phys. **104**, 6755 (1996).
[71] P. Bolhuis and D. Frenkel, J. Chem. Phys. **106**, 666 (1997).
[72] A. Poniewierski, Phys. Rev. A **45**, 5605 (1992).
[73] M. Marechal, U. Zimmermann, and H. Löwen, J. Chem. Phys. **136**, 144506 (2012).